

**THE EXAMINATION OF NEW EQUIVALENT EDGE
CURRENTS IN THE PREDICTION OF HIGH
FREQUENCY BACKSCATTERING FROM FLAT
PLATES**

A THESIS

**Submitted To The Department Of Electrical And
Electronics Engineering
And The Institute Of Engineering And Sciences
Of Bilkent University
In Partial Fulfillment Of The Requirements
For The Degree Of
Master Of Science**

By

Taner OĞUZER

September 1991

**QC
665
.D5
039
1991**

THE EXAMINATION OF NEW EQUIVALENT EDGE
CURRENTS IN THE PREDICTION OF HIGH
FREQUENCY BACKSCATTERING FROM FLAT
PLATES

A THESIS

SUBMITTED TO THE DEPARTMENT OF ELECTRICAL AND
ELECTRONICS ENGINEERING
AND THE INSTITUTE OF ENGINEERING AND SCIENCES
OF BILKENT UNIVERSITY
IN PARTIAL FULFILLMENT OF THE REQUIREMENTS
FOR THE DEGREE OF
MASTER OF SCIENCE

By

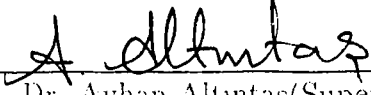
Taner Oğuzer

September 1991

Taner Oğuzer
tarafından hazırlanmıştır.

OL
665
.D5
O 39
1991
B. 9329

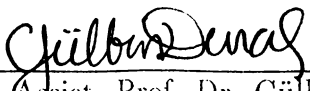
I certify that I have read this thesis and that in my opinion it is fully adequate, in scope and in quality, as a thesis for the degree of Master of Science.


Assoc. Prof. Dr. Ayhan Altıntaş(Supervisor)

I certify that I have read this thesis and that in my opinion it is fully adequate, in scope and in quality, as a thesis for the degree of Master of Science.


Prof. Dr. Abdullah Atalar

I certify that I have read this thesis and that in my opinion it is fully adequate, in scope and in quality, as a thesis for the degree of Master of Science.


Assist. Prof. Dr. Gülbin Dural

Approved for the Institute of Engineering and Sciences:


Prof. Dr. Mehmet Baray
Director of Institute of Engineering and Sciences

ABSTRACT

THE EXAMINATION OF NEW EQUIVALENT EDGE CURRENTS IN THE PREDICTION OF HIGH FREQUENCY BACKSCATTERING FROM FLAT PLATES

Taner Oğuzer

M.S. in Electrical and Electronics Engineering

Supervisor: Assoc. Prof. Dr. Ayhan Altıntaş

September 1991

Equivalent edge currents based on the geometrical theory of diffraction (GTD) have been utilized for the prediction of electromagnetic scattering from edged bodies. These equivalent currents are use Keller's diffraction coefficient and therefore not valid for arbitrary aspect of observation. More general expressions for equivalent edge currents are later obtained by Michaeli. Those expressions become infinite at certain observation directions. These infinities are later eliminated by the same author for the fringe component of the equivalent currents by choosing a skew coordinate system on the half plane to be used for the asymptotic integration.

A similar approach is employed here to eliminate the infinities in the physical optics(PO) component of the equivalent edge currents. It is also shown that the radiation from the fringe and PO equivalent currents is unique and yields the GTD field.

The fringe and PO equivalent currents are then applied to the backscattering problems from the perfectly conducting square and triangular plates. The higher order interactions between the edges are also included into the analysis. Some improvements are obtained over the previous solutions.

Keywords: Electromagnetic backscattering, radar cross section, equivalent edge currents.

ACKNOWLEDGMENT

I would like to express my deep gratitude to Assoc. Prof. Dr. Ayhan Altıntaş for his suggestions, helps and invaluable guidance during the development of this thesis.

I want to thank to my family for their constant support and to all my friends, especially Atilla Malaş, Erkan Savran and Fırat Kılıç.

ÖZET

DÜZLEMSEL PLAKALARDAN GERİ SAÇINIMIN HESAPLANMASINDA YENİ EŞDEĞER KENAR AKIMLARININ KULLANILMASI

Taner Oğuzer

Elektrik ve Elektronik Mühendisliği Bölümü Yüksek Lisans

Tez Yöneticisi: Doç. Dr. Ayhan Altıntaş

Eylül 1991

Kenarlı cisimlerden yayılan elektromanyetik saçınımın tahmin edilmesi amacıyla kırınımın geometrik kuramı(KGK)'na dayanan eşdeğer kenar akımları kullanılmaktaydı. KGK'dan elde edilen bu akımlar bütün gözlem doğrultularında geçerli değildi. Daha sonra, Michaeli eşdeğer kenar akımlarını daha genel bir yoldan elde etti. Fakat bu akımlar pekçok gözlem doğrultusu için sonsuzluklara sahipti. Michaeli, eşdeğer kenar akımlarının artık kısmı için bu sonsuzlukları yarı düzlemin üzerinde seçilen eğik bir koordinat sistemi ile yok edebildi.

Bu çalışmada, benzeri bir yaklaşım eşdeğer kenar akımlarının fiziksel optik(FO) kısmındaki sonsuzlukları yok edebilmek amacıyla kullanıldı. Ayrıca, eşdeğer artık ve FO akımlarının yarattığı ışınımın KGK sonucunu verdiği gözlemlendi.

Yeni eşdeğer akımlar, mükemmel iletken kare ve üçgen düzlemsel plakalardan geri saçınımın bulunması için kullanıldı. Elde edilen sonuçların önceki verilerle karşılaştırılması bazı ilerlemelerin elde edildiğini gösterdi.

Anahtar sözcükler: Elektromanyetik geri saçınım, radar yüzey kesiti, eşdeğer kenar akımları.

Contents

1	INTRODUCTION	1
2	THE GEOMETRICAL THEORY OF DIFFRACTION	4
2.1	Introduction	4
2.2	Geometrical Theory of Diffraction	6
2.3	Uniform Geometrical Theory of Diffraction	8
3	EQUIVALENT CURRENT METHOD	10
3.1	Introduction	10
3.2	Equivalent Edge Currents For Arbitrary Aspects of Observation	13
3.2.1	Half Plane	16
3.2.2	Fringe Component of Equivalent Edge Currents	17
3.3	Derivation of PO Equivalent Edge Currents For a Half Plane . .	20
3.4	Higher Order Equivalent Currents	24
4	BACK SCATTERING FROM FLAT PLATES	27
4.1	Square Plate	28
4.1.1	E-Polarization	31
4.1.2	H-polarization	32
4.2	Triangular Plate	34

<i>CONTENTS</i>	vii
4.2.1 E-Polarization	37
4.2.2 H-Polarization	41
5 COMPARISON OF THE RESULTS	42
6 CONCLUSIONS	52
A Radiation From The Infinite Line Sources	53

List of Figures

2.1	An astigmatic ray tube	5
2.2	Perfectly conducting wedge	5
2.3	Cone of Diffracted Rays	7
2.4	Transition Function	9
3.1	Radiation of Equivalent Currents	11
3.2	Diffraction by an infinite wedge	12
3.3	A Perfectly Conducting Flat Surface	14
3.4	Two dimensional view at the diffraction point Q	14
3.5	Perfectly conducting half plane	16
3.6	Singularity Cones	18
3.7	Skew Coordinate System	21
3.8	Edge interactions in a flat plate	25
4.1	Perfectly Conducting Square Plate	29
4.2	Edge Interactions in the Square Plate	33
4.3	Perfectly Conducting Triangular Plate	35
4.4	Edge interactions in the triangular plate	39
5.1	Backscattering from the square plate: II-pol ($a=3.125\lambda$)	44

5.2	Backscattering from the square plate: E-pol ($a=3.125\lambda$)	45
5.3	Backscattering from triangular plate: E-pol($a=4\lambda$, $\text{alfa}=60\text{deg}$) .	46
5.4	Backscattering from triangular plate: E-pol($a=4\lambda$, $\text{alfa}=45\text{deg}$) .	47
5.5	Backscattering from triangular plate: E-pol($a=4\lambda$, $\text{alfa}=90\text{deg}$) .	48
5.6	Backscattering from triangular plate: E-pol($a=3\lambda$, $\text{alfa}=30\text{deg}$) .	49
5.7	Backscattering from triangular plate: H-pol($a=4\lambda$, $\text{alfa}=45\text{deg}$)	50
5.8	Backscattering from triangular plate: H-pol($a=9\lambda$, $\text{alfa}=30\text{deg}$)	51
A.1	Infinite line sources	53

Chapter 1

INTRODUCTION

The electromagnetic scattering is the result of the obstruction of the electromagnetic field by an object. The scattered field is defined as the difference between the field in the presence of the object and the field that would exist if the object were absent.

An important parameter in scattering that is widely used in the radar applications is the radar cross section. Radar cross section of a target is the area intercepting that amount of power which, when scattered equally in all directions, produces an echo at the radar equal to that from the target. In other words,

$$\sigma = \lim_{R \rightarrow \infty} 4\pi R^2 \left| \frac{E^s}{E^i} \right|^2 \quad (1.1)$$

where R is the distance between radar and target. E^s and E^i are the scattered and the incident field strengths at the observation point. If the scattered field is observed in the incident direction; i.e. the backscattering case, then σ is called the monostatic radar cross section.

In theory, the scattered field can be determined by solving Maxwell's equations subject to appropriate boundary conditions. Unfortunately, analytical solutions of Maxwell's equations is limited to only simple shapes. Therefore, construction of the integral equations and their numerical solutions became considerably popular. These numerical solutions are generally quite accurate when the objects are not too large with respect to the wavelength.

When the size of the object is large, high frequency ray optical techniques are used for the approximate solution of the scattering problems. The simplest ray optical approach is the geometrical optics (GO), in which the high

frequency electromagnetic field is assumed to propagate along ray paths which satisfy Fermat's principle and the next wavefront of the field can be determined from the preceding one by tracing rays.

To obtain more accurate high frequency results, an asymptotic high frequency technique which is an extension of GO were developed in 1962 by Keller[1]. It is called the Geometrical Theory of Diffraction (GTD). In GTD, the known exact analytical solution for the problem of scattering from simple shapes, called canonical problems, are analyzed asymptotically for high frequencies. The GO and diffraction ray contributions are then identified from the asymptotic expressions.

On the other hand, it is seen that the ray theory fails around the caustic directions. To correct the scattered field, an Equivalent Current Method (ECM)[3] was developed and applied to the scattering problems in caustic directions. But these equivalent currents use Keller's diffraction coefficient and therefore not valid for arbitrary aspect of observation.

More general expressions for equivalent edge currents are later obtained by Michaeli[5]. Unfortunately, those expressions become infinite at certain observation directions. In a subsequent paper[7], Michaeli considered these currents as arising separately from physical optics(PO) and fringe components and showed that for the fringe component the infinities can be eliminated by choosing a proper skew coordinate system for the asymptotic integration. However, it was asserted by the same author[8] that the infinities in the PO component cannot be eliminated in a similar way. On the other hand, the PO equivalent edge currents which are free from infinities are obtained by an application of the Stokes' theorem for a finite size flat plate in [6].

In the present study, similar to the approach in [7], the PO equivalent currents are derived for a half plane by using a different selection of the skew coordinate over the surface. Then it is shown that the total radiation from the fringe and PO equivalent currents yields the GTD field. In addition, it is observed that the obtained PO equivalent currents are the same with the ones obtained in [6]. The new fringe and PO equivalent currents are then applied to the backscattering problem from the square and triangular plates. The equivalent currents are also combined with UTD to involve the multiple diffraction mechanisms between the edges into the analysis. Finally, the results are compared with the previous works of Sitka[9], Ross[10] and the measured data[9].

The outline of the thesis is as follows. The GTD is introduced in chapter 2. In chapter 3, Equivalent Current Method is described. The fringe and PO equivalent current components are derived for a half plane and the computation of higher order diffractions using equivalent currents is explained. In chapter 4, the derived equivalent currents with the higher order diffractions are applied to the backscattering from the square and triangular plates. E and H polarization cases are analyzed separately. In chapter 5, the results obtained in chapter 4 are compared with the previous work and measured data. Finally, conclusions are given in chapter 6.

In the analysis, a sinusoidally-varying time dependence $e^{j\omega t}$ is assumed and suppressed.

Chapter 2

THE GEOMETRICAL THEORY OF DIFFRACTION

2.1 Introduction

In GO, propagation of field from one point to another, in an isotropic lossless medium, is determined by using the conservation of energy flux in a tube of ray as shown in Figure 2.1. The phase of the field is determined by optical length from a reference point and the phase constant of the medium. Then the GO field,

$$\mathbf{E}(s) = \mathbf{E}(s = o)e^{-jk\psi(o)} \sqrt{\frac{\rho_1 \rho_2}{(\rho_1 + s)(\rho_2 + s)}} e^{-jks} \quad (2.1)$$

where ρ_1 and ρ_2 are the principal radii of curvature of the wavefront at the reference point. s is the distance along the ray path.

A wedge consists of two perfectly conducting half planes intersecting at a straight edge as shown in Figure 2.2. At high frequencies, the total electric field is given by

$$\mathbf{E} = \mathbf{E}^i \mathbf{u}^i + \mathbf{E}^r \mathbf{u}^r + \mathbf{E}^d \quad (2.2)$$

In this representation, the source and the field points are sufficiently removed from the wedge surface. \mathbf{E}^i is the electric field of the source in the absence of the surface, \mathbf{E}^r is the electric field reflected from the illuminated surface with the edge ignored and \mathbf{E}^d is the edge diffracted electric field. \mathbf{E}^i and \mathbf{E}^r are the GO fields and \mathbf{u}^i and \mathbf{u}^r are the illumination regions determined by GO as follows:

$$\mathbf{u}^i = \begin{cases} 1 & 0 < \phi < \pi + \phi' \\ 0 & \pi + \phi' < \phi < n\phi \end{cases} \quad (2.3)$$

$$\mathbf{u}^r = \begin{cases} 1 & 0 < \phi < \pi - \phi' \\ 0 & \pi - \phi' < \phi < n\phi \end{cases} \quad (2.4)$$

where ϕ' and ϕ are the incidence and diffraction angles respectively as defined in Figure 2.2.

2.2 Geometrical Theory of Diffraction

GTD is based on the following three postulates;

a) Diffraction like reflection is a local phenomenon at high frequencies.

b) The diffracted ray and the corresponding incident ray make equal angles with the edge at the point of diffraction (See Fig 2.3). Hence the diffracted rays propagate on a cone that is called the Keller Cone. This is the result of the generalized Fermat's principle.

c) Away from the point of diffraction, the diffracted rays behave like GO rays.

Therefore the edge diffracted field away from the edge is given by

$$\mathbf{E}^d(s) = \mathbf{E}^d(O) \sqrt{\frac{\rho\rho'}{(\rho+s)(\rho'+s)}} e^{-jks} \quad (2.5)$$

where ρ and ρ' are the principle radii of curvature of the diffracted field wavefront at the reference point O. When the reference point becomes at the edge point Q_E , then the diffracted field is proportional to the field incident at Q_E .

$$\lim_{\rho' \rightarrow \infty} \vec{\mathbf{E}}^d(O) \sqrt{\rho'} = \vec{\mathbf{E}}^i(Q_E) \cdot \vec{\mathbf{D}} \quad (2.6)$$

where $\vec{\mathbf{D}}$ is the dyadic edge diffraction coefficient. Then the edge diffracted electric field

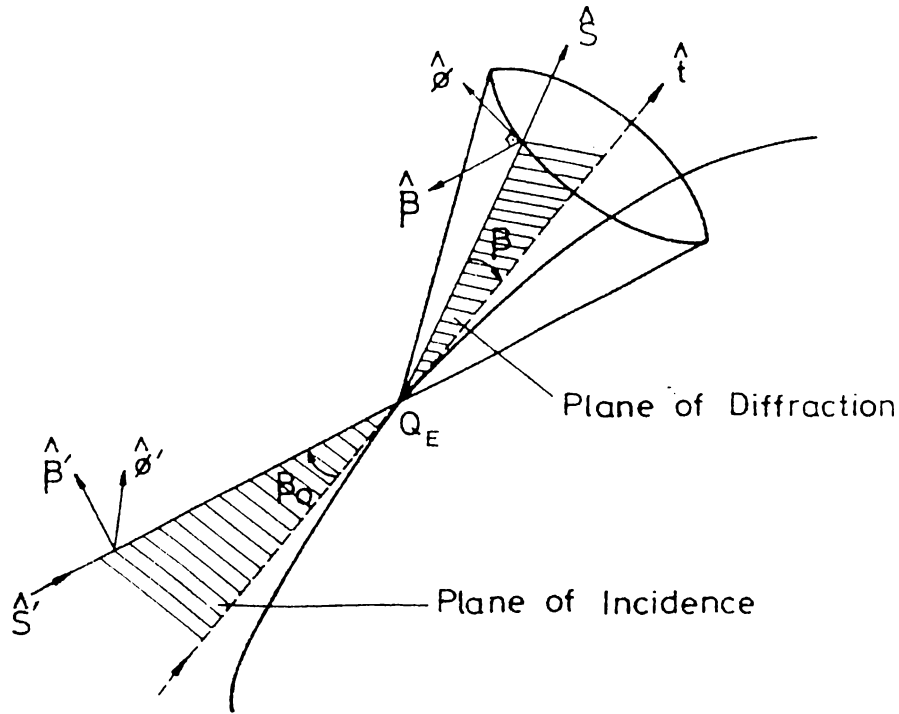


Figure 2.3: Cone of Diffracted Rays

$$\vec{\mathbf{E}}^d(s) = \vec{\mathbf{E}}^i(Q_E) \cdot \bar{\bar{D}} \sqrt{\frac{\rho_c}{s(s + \rho_c)}} e^{-jks} \quad (2.7)$$

in which ρ_c is the distance between the caustic at the edge and the caustic of the diffracted ray. For straight edges and plane wave incidence, it becomes that

$$\vec{\mathbf{E}}^d = \vec{\mathbf{E}}^i(Q_E) \cdot \bar{\bar{D}} \frac{e^{-jks}}{\sqrt{s}} \quad (2.8)$$

In a ray fixed coordinate system, $\bar{\bar{D}}$ is a 2×2 matrix. In this case, the unit vectors $\hat{\phi}$ and $\hat{\phi}'$ are perpendicular to the plane of incidence and the unit vectors $\hat{\beta}$ and $\hat{\beta}'$ are parallel to the plane of incidence and the plane of diffraction respectively. \hat{s} and \hat{s}' are the unit vectors in the directions of incidence and diffraction respectively as shown in Figure 2.3. Then, for plane wave incidence, the diffracted field can be written as

$$\begin{bmatrix} \mathbf{E}_\beta^d \\ \mathbf{E}_\phi^d \end{bmatrix} = - \begin{bmatrix} D_s & \mathbf{O} \\ \mathbf{O} & D_h \end{bmatrix} \frac{e^{-jks}}{\sqrt{s}} \quad (2.9)$$

where D_s and D_h are the diffraction coefficients for the soft and hard boundary conditions. They are first obtained by Keller for a wedge as

$$D_{\text{h}} = \frac{e^{-j\pi/4}}{\sqrt{2\pi k \sin \beta}} [G(\phi - \phi') \bar{+} G(\phi + \phi')] \quad (2.10)$$

where

$$G(\beta) = \frac{1/n \sin \pi/n}{\cos \pi/n - \cos \beta/n} \quad (2.11)$$

and n is the measure of the wedge angle as in Figure 2.2.

2.3 Uniform Geometrical Theory of Diffraction

GO fields show a sharp discontinuity at the incident and reflection boundaries. Unfortunately, Keller's diffraction coefficients predict infinite values at the shadow boundaries (See Figure 2.2). Therefore the diffracted field must be modified to make the total field smooth and continuous. In UTD, uniform diffraction coefficients are obtained as [2]

$$D_{\text{h}} = D(L, \beta^-, n) \bar{+} D(L, \beta^+, n) \quad (2.12)$$

where

$$D(L, \beta, n) = -\frac{e^{-j\pi/4}}{2n\sqrt{2\pi k \sin \beta}} \left[\cot\left(\frac{\pi + \beta}{2n}\right) \mathbf{F}[kLa^+(\beta)] + \cot\left(\frac{\pi - \beta}{2n}\right) \mathbf{F}[kLa^-(\beta)] \right] \quad (2.13)$$

and $\mathbf{F}(x)$ is the transition function which has a Fresnel integral as follows

$$\mathbf{F}(x) = 2j\sqrt{x}e^{jx} \int_{\sqrt{x}}^{\infty} e^{-j\tau^2} d\tau \quad (2.14)$$

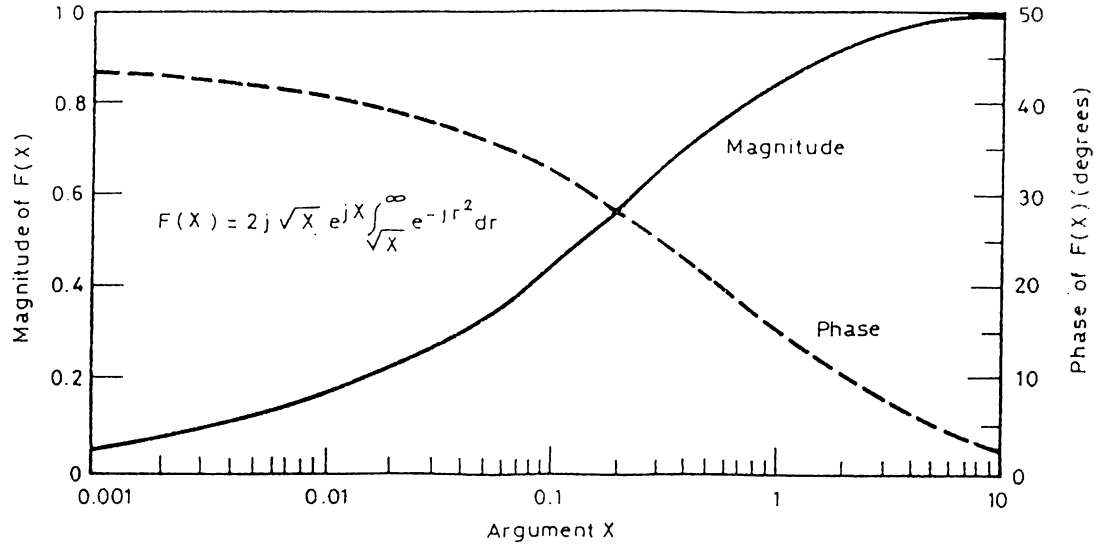


Figure 2.4: Transition Function

The magnitude and phase variations of the transition function are shown in Figure 2.4. The parameters $a^{\pm}(\beta)$ are determined as follow:

$$a^{\pm}(\beta) = 2 \cos^2\left(\frac{2n\pi N^{\pm} - \beta}{2}\right) \quad (2.15)$$

where N^{\pm} are the integers which most nearly satisfy the following equations:

$$2\pi n N^+ - \beta = \pi \quad (2.16)$$

$$2\pi n N^- - \beta = -\pi \quad (2.17)$$

with $\beta^{\pm} = \phi^{\pm} - \phi'$ and $L = s \sin^2 \beta$ for plane wave incidence.

More details of UTD and diffraction coefficients are explained in [2].

Chapter 3

EQUIVALENT CURRENT METHOD

3.1 Introduction

In contrast to diffraction by straight edges, edge diffracted fields from three dimensional objects may have caustics. It is known that GTD or its modifications fail around the directions of ray caustics. To overcome this failure of ray theory, an Equivalent Current Method (ECM) incorporated with the GTD was proposed by Ryan and Peters in 1969[3].

The idea of equivalent current concept consists of determining the equivalent electric and magnetic type currents flowing along the edge of a wedge which produce the actual diffracted field of the wedge when radiate in the absence of the wedge. Then, the edge diffracted field for an arbitrary scatterer can be found by the following radiation integral. (See Figure 3.1)

$$\vec{E}^s = \frac{jkZ}{4\pi} \frac{e^{-jkR}}{R} \int_C [\hat{R} \times \hat{R} \times \hat{I} + Y \hat{R} \times \hat{M}] e^{jk\hat{R} \cdot \hat{r}'} dl \quad (3.1)$$

where I and M are the equivalent electric and magnetic type currents in the place of the diffracting edge of the scatterer. Z and Y are the impedance and admittance of free space. C , as in Figure 3.1, represents the contour along the edge of the scatterer. \hat{R} is the unit vector in the direction of observation.

Away from the caustic regions, the above integral is evaluated using stationary phase arguments. The stationary phase points are the diffraction points and the value of the expression in(3.1) should give the diffracted fields as calculated by the GTD.

By comparing the stationary value of the integral with the GTD fields, one

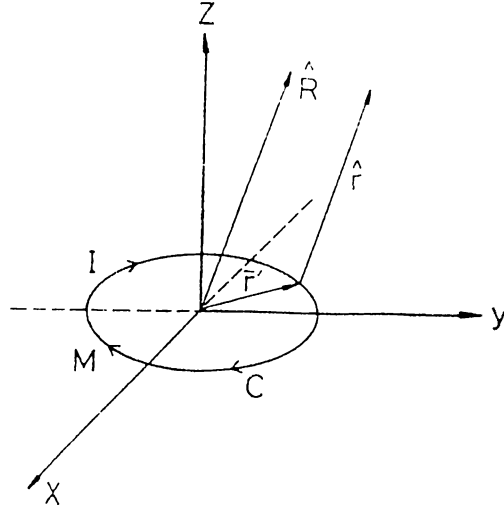


Figure 3.1: Radiation of Equivalent Currents

obtains the equivalent currents as

$$\mathbf{I} = -Y \sqrt{\frac{8\pi}{k}} e^{-j\pi/4} D_s \frac{E_{tan}^i}{\sin \beta_o} \hat{t} \quad (3.2)$$

$$\mathbf{M} = -Z \sqrt{\frac{8\pi}{k}} e^{-j\pi/4} D_h \frac{H_{tan}^i}{\sin \beta_o} \hat{t} \quad (3.3)$$

where E_{tan}^i and H_{tan}^i are the incident electric and magnetic fields tangential to the edge at the diffraction point and \hat{t} is the unit vector along the edge. D_s and D_h are the soft and hard diffraction coefficients. β_o is the oblique incident angle as shown in Figure 3.2.

Since these equivalent currents are derived from the GTD fields, they are only valid on the Keller Cone ($\beta = \beta_o$). As a consequence of this restriction, equivalent currents cannot be used for arbitrary direction of observation. Therefore to extend applicability of equivalent currents to include the directions which are not on the Keller Cone, an arbitrary diffraction angle β is needed as well as the incident angle β_o in the expressions of the equivalent currents. (See Figure 3.2)

For this purpose, Knott and Senior[4], on the basis of reciprocity considerations, proposed the following replacement

$$\sin \beta_o = \sqrt{\sin \beta \sin \beta_o} \quad (3.4)$$

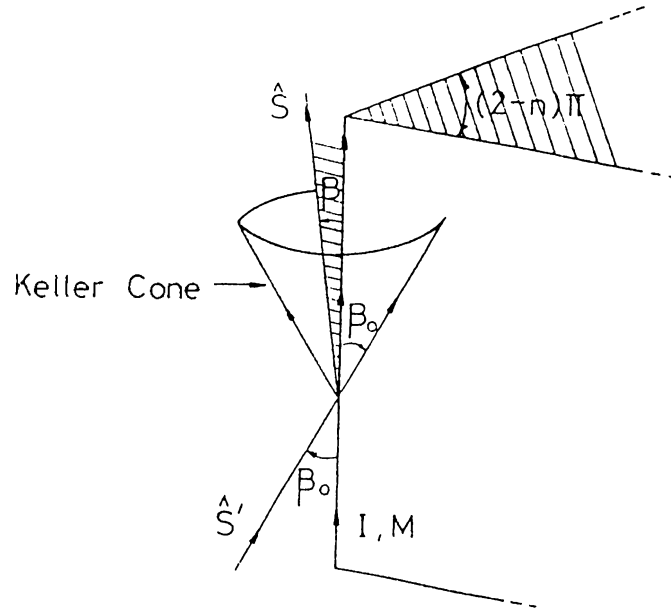


Figure 3.2: Diffraction by an infinite wedge

and accordingly, they modified the equivalent edge currents as follows:

$$\mathbf{I} = -Y \sqrt{\frac{8\pi}{k}} \frac{e^{-j\pi/4}}{\sqrt{\sin \beta \sin \beta_0}} D_s E_{\tan}^i \hat{t} \quad (3.5)$$

$$\mathbf{M} = -Z \sqrt{\frac{8\pi}{k}} \frac{e^{-j\pi/4}}{\sqrt{\sin \beta \sin \beta_0}} D_h H_{\tan}^i \hat{t} \quad (3.6)$$

Although these expressions are consistent with the reciprocity principle, their derivation is not based on mathematical grounds.

To obtain the equivalent edge currents for arbitrary direction of observation, a new approach is suggested by Michaeli[5]. He proposed that the equivalent current expressions can be derived from the asymptotic integration of surface currents. This new asymptotic method is explained in the next section.

3.2 Equivalent Edge Currents For Arbitrary Aspects of Observation

Consider a perfectly conducting flat surface S on the xy -plane with an edge C as shown in Figure 3.3. At any point on the edge, the unit vector \hat{l} is tangent to the edge, \hat{n} is normal to the surface, and the binormal unit vector is given by

$$\hat{b} = \hat{n} \times \hat{l} \quad (3.7)$$

The angles ϕ , ϕ' , β and β' are measured as shown in Figures 3.3 and 3.4. R is the distance to the observation point measured from the origin at the coordinate system. \hat{s}' and \hat{s} are the unit vectors for incident and observation directions. The far scattered field from this structure is given with the following radiation integral.

$$\hat{E}^s = \frac{jkZ}{4\pi} \frac{e^{-jkR}}{R} \hat{s}' \times \hat{s} \times \int \int_S \hat{J}_T(x, y) e^{j(k_x x + k_y y)} ds \quad (3.8)$$

where Z is the intrinsic impedance, k is the wavenumber and $\hat{J}_T(x, y)$ is the total induced current on the conducting surface. In addition, k_x and k_y are given by

$$k_x = k \hat{s} \cdot \hat{x} \quad (3.9)$$

$$k_y = k \hat{s} \cdot \hat{y} \quad (3.10)$$

If the field point is not on a caustic of reflected field, then in the limit $k \rightarrow \infty$, the surface radiation integral can be reduced asymptotically to a sum of field contributions from an interior stationary point on S and a boundary contribution expressed by a line integral C . The former gives the reflected field and the latter should represent the edge diffracted field.

Then, the edge diffracted field in (t, b) coordinate system is given by

$$\hat{E}^d = \frac{jkZ}{4\pi} \frac{e^{-jkR}}{R} \hat{s}' \times \hat{s} \times \int_C \int_o \hat{J}_T(t, b) e^{jk(b\hat{b} \cdot \hat{s} + t\hat{i} \cdot \hat{s})} db dt \quad (3.11)$$

where "o" denotes the asymptotic end-point contribution at $b=0$.

Let

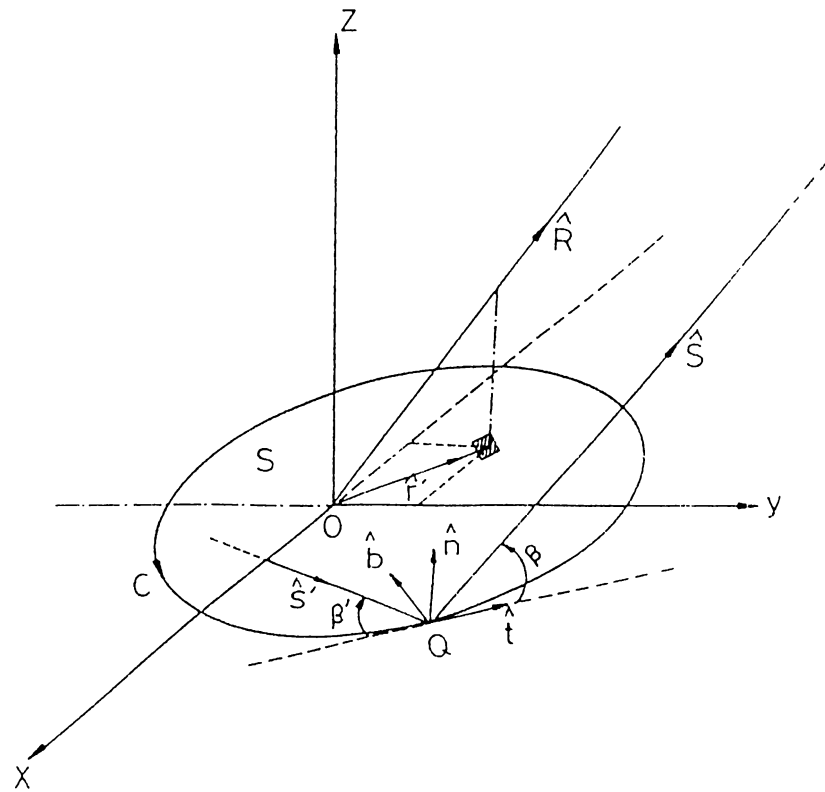


Figure 3.3: A Perfectly Conducting Flat Surface

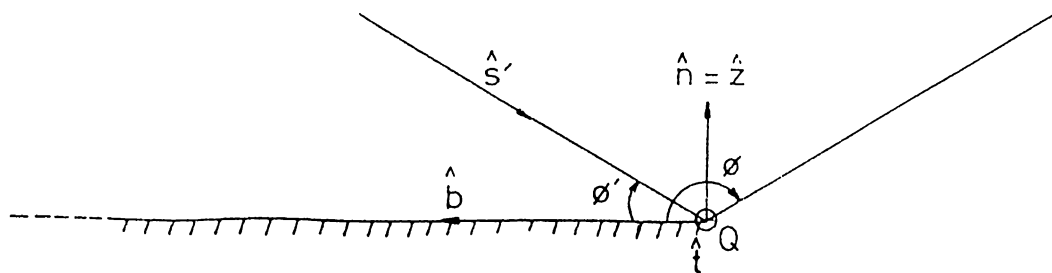


Figure 3.4: Two dimensional view at the diffraction point Q

$$\vec{K}(t) = \int_{\mathcal{C}} \hat{J}_T(t, b) e^{jk\hat{b}\hat{s}} db \quad (3.12)$$

Then

$$\hat{E}^d = \frac{jkZ}{4\pi} \frac{e^{-jkR}}{R} \hat{s} \times \hat{s} \times \int_{\mathcal{C}} \vec{K}(t) e^{jkt\hat{s}} dt \quad (3.13)$$

The edge diffracted field can also be expressed as due to the equivalent edge currents along the edge

$$\hat{E}^d = \frac{jkZ}{4\pi} \frac{e^{-jkR}}{R} \int_{\mathcal{C}} [\hat{s} \times \hat{s} \times \hat{I} + Y \hat{s} \times \hat{I} \mathbf{M}] e^{jkt\hat{s}} dt \quad (3.14)$$

Equating the two integrands, we have

$$Z \hat{s} \times \hat{s} \times \vec{K} = Z \mathbf{I} \hat{s} \times \hat{s} \times \hat{I} + \mathbf{M} \hat{s} \times \hat{I} \quad (3.15)$$

Dot multiplying both sides of the equations with $\hat{s} \times \hat{I}$ and $\hat{s} \times \hat{s} \times \hat{I}$,

$$\mathbf{I} = \frac{1}{\sin^2 \beta} \hat{s} \cdot [(\hat{I} \times \hat{s}) \times \vec{K}] \quad (3.16)$$

$$\mathbf{M} = \frac{Z}{\sin^2 \beta} \hat{I} \cdot (\hat{s} \times \vec{K}) \quad (3.17)$$

are obtained.

Finally, by using

$$\hat{s} = \hat{t} \cos \beta + \hat{b} \sin \beta \cos \phi + \hat{n} \sin \beta \sin \phi \quad (3.18)$$

expressions change to

$$\mathbf{I} = K_t - K_b \cot \beta \cos \phi \quad (3.19)$$

$$\mathbf{M} = -Z \frac{\sin \phi}{\sin \beta} K_b \quad (3.20)$$

where K_t and K_b are the tangential and binormal components of the vector \vec{K} .

3.2.1 Half Plane

Let a perfectly conducting half plane is illuminated by a plane wave as shown in Figure 3.4.

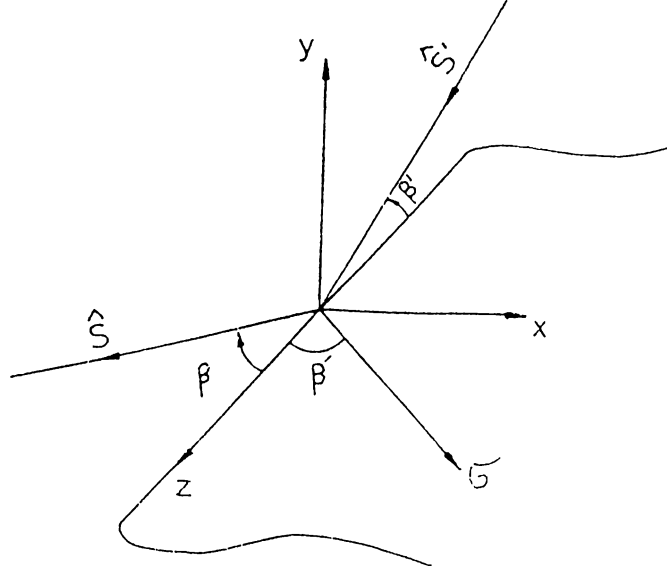


Figure 3.5: Perfectly conducting half plane

The local edge unit vectors are given by $\hat{n} = \hat{y}$, $\hat{b} = \hat{x}$ and $\hat{t} = \hat{z}$. ϕ , ϕ' , β and β' are the same as shown in Figures 3.3 and 3.4.

If the incident field is given by

$$\vec{E}^i = (\hat{\beta}' + \hat{\phi}') e^{jk(x \sin \beta' \cos \phi' + y \sin \beta' \sin \phi' - z \cos \beta')} \quad (3.21)$$

$$\vec{H}^i = Y \hat{s}' \times \vec{E}^i \quad (3.22)$$

Using UTD, the total magnetic field is given by

$$\vec{H}_T = \vec{H}_{GO} + \vec{H}_{UTD}^t \quad (3.23)$$

Then the total surface current density is found from

$$\vec{J}_T = \hat{n} \times [\vec{H}_T(\phi = 0) - \vec{H}_T(\phi = 2\pi)] \quad (3.24)$$

which can be decomposed as

$$\vec{J}_T = (J_x^{GO} + J_x^f)\hat{x} + (J_z^{GO} + J_z^f)\hat{z} \quad (3.25)$$

where

$$J_x^{GO} = 2Y \sin \beta' e^{-jkz \cos \beta'} e^{-jkx \sin \beta' \cos \phi'} \quad (3.26)$$

$$\begin{aligned} J_z^{GO} &= -2Y \cos \phi' \cos \beta' e^{jkx \sin \beta' \cos \phi'} \\ &+ 2Y \sin \phi' e^{jkx \sin \beta' \cos \phi'} e^{-jkz \cos \beta'} \end{aligned} \quad (3.27)$$

and

$$J_x^f = -4Y \sin \beta' \frac{e^{j\pi/4}}{\sqrt{\pi}} e^{-jkz \cos \beta'} e^{jkx \sin \beta' \cos \phi'} \int_{\sqrt{2kx \sin \beta'}}^{\infty} e^{-j\tau^2} d\tau \quad (3.28)$$

$$\begin{aligned} J_z^f &= 4Y \frac{e^{j\pi/4}}{\sqrt{\pi}} \cos \beta' \cos \phi' e^{jkx \sin \beta' \cos \phi'} e^{-jkz \cos \beta'} \int_{\sqrt{2kx \sin \beta'}}^{\infty} e^{-j\tau^2} d\tau \\ &+ -4Y \sin \phi' \frac{e^{j\pi/4}}{\sqrt{\pi}} e^{jkx \sin \beta' \cos \phi'} e^{-jkz \cos \beta'} \int_{\sqrt{2kx \sin \beta'}}^{\infty} e^{-j\tau^2} d\tau \\ &+ 2Y e^{-j\pi/4} \sqrt{\frac{2}{kx\pi \sin \beta'}} \cos \beta' \cos \phi' / 2 e^{-jkx \sin \beta'} e^{-jkz \cos \beta'} \\ &+ 2Y e^{-j\pi/4} \sqrt{\frac{2}{kx\pi \sin \beta'}} \sin \phi' / 2 e^{-jkx \sin \beta'} e^{-jkz \cos \beta'} \end{aligned} \quad (3.29)$$

J^{GO} is the geometrical optics approximation to the current density and J^f is the fringe or "non-uniform" component as named by Ufimtsev. We will examine the radiation of each component separately.

3.2.2 Fringe Component of Equivalent Edge Currents

The derivation of the fringe component of the equivalent edge currents requires the asymptotic end-point evaluation of the following integral.

$$\vec{K}^f(z) = \int_0^{\infty} \vec{J}^f(x, z) e^{jkx\hat{x}\cdot\hat{s}} dx \quad (3.30)$$

Fringe current $\vec{J}^f(x, z)$ can not be represented near the edge($x=0$) in a simple amplitude-phase form. However, away from the edge, GTD gives a phase as $-kx\hat{x} \cdot \hat{\sigma}$. This phase describes $\vec{J}^f(x, z)$ as a wave propogating in the $\hat{\sigma}$ direction which is the direction of diffracted rays at the intersection of Keller cone with the half plane. Thus if it is assumed that the ray behaviour of the fringe surface field is valid up to very close edge, then the integral in (3.31) becomes infinite, if the following condition holds

$$\hat{s} \cdot \hat{x} = \hat{\sigma} \cdot \hat{x} \tag{3.31}$$

In other words, the singularity condition is satisfied when the phase of $\vec{J}^f(x, z)$ cancels the phase of the exponent in the integral. This singularity condition represents a cone around the x-axis as shown in Figure 3.6. With this argument, Michaeli[7] stated that these expected singularities can be reduced to a single direction by choosing a proper skew coordinate system. Therefore σ and z coordinates are selected instead of the cartesian coordinates x and z with the following relations.

$$x = \sigma \sin \beta' \tag{3.32}$$

$$z = z + \sigma \sin \beta' \tag{3.33}$$

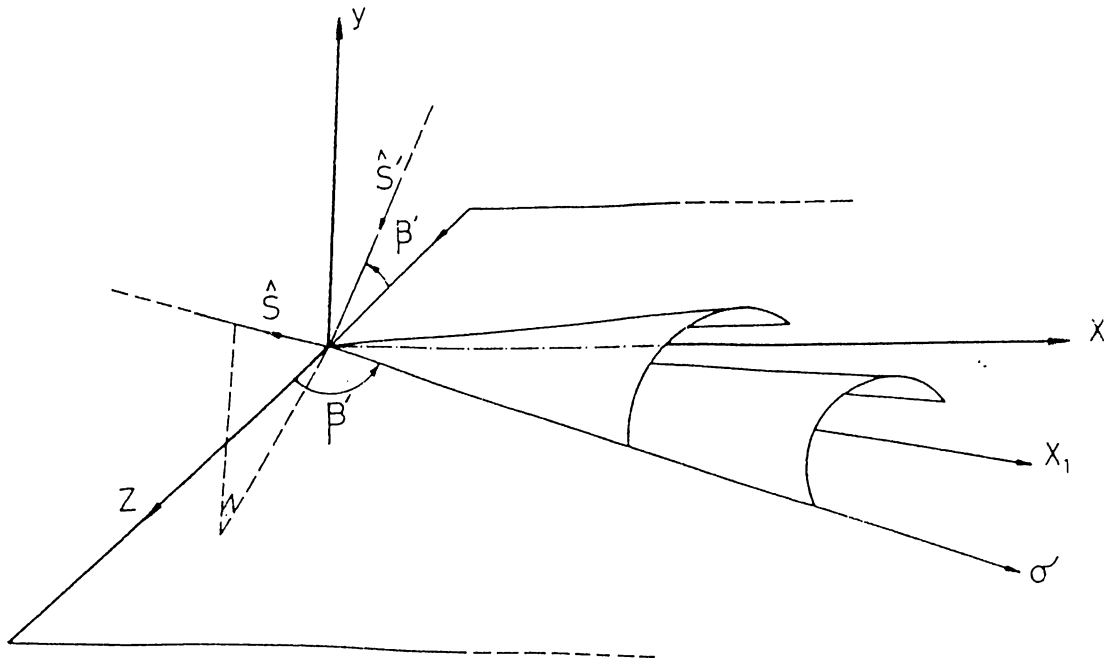


Figure 3.6: Singularity Cones

Using the new coordinates, the integration becomes

$$\vec{K}^J(z) = \sin \beta' \int_0^1 \vec{J}^J(\sigma \sin \beta', z + \sigma \cos \beta') e^{jk\sigma \hat{\sigma} \cdot \hat{s}} d\sigma \quad (3.34)$$

By substituting the $\vec{K}^J(z)$ into the equations (3.19) and (3.20), this yields the following fringe current components.

$$\mathbf{I}^J = Y E_{tan}^i d_s^J + H_{tan}^i d_2^J \quad (3.35)$$

$$\mathbf{M}^J = Z H_{tan}^i d_h^J \quad (3.36)$$

The variables d_s^J, d_2^J and d_h^J are defined by

$$d_s^J = \frac{-2\sqrt{2}}{jk} \frac{\sin \phi'/2 (\sqrt{F(\beta', \beta, \phi)} - \sqrt{2} \sin \beta' \cos \phi'/2)}{\sin \beta' G(\beta', \beta, \phi', \phi)} \quad (3.37)$$

$$d_2^J = \frac{2}{jk} \frac{\sin \beta' (\cot \beta \cos \phi + \cot \beta' \cos \phi' + \cos \phi'/2 \sqrt{\frac{2}{F(\beta', \beta, \phi)}} H(\beta', \beta, \phi))}{G(\beta', \beta, \phi', \phi)} \quad (3.38)$$

$$d_h^J = \frac{-2}{jk} \frac{\sin \beta' \sin \phi (1 - \sin \beta' \cos \phi'/2 \sqrt{\frac{2}{F(\beta', \beta, \phi)}})}{\sin \beta G(\beta', \beta, \phi', \phi)} \quad (3.39)$$

where

$$\begin{aligned} F(\beta', \beta, \phi) &= \sin \beta' (\sin \beta' - \sin \beta \cos \phi) \\ &\quad - \cos \beta' (\cos \beta - \cos \beta') \end{aligned} \quad (3.40)$$

$$\begin{aligned} G(\beta', \beta, \phi', \phi) &= \sin \beta' (\sin \beta \cos \phi + \sin \beta' \cos \phi') \\ &\quad + \cos \beta' (\cos \beta - \cos \beta') \end{aligned} \quad (3.41)$$

$$\begin{aligned} H(\beta', \beta, \phi) &= \cot \beta' [\sin \beta \cos \phi + \cot \beta' (\cos \beta - \cos \beta')] \\ &\quad - \sin \beta' \cot \beta \cos \phi \end{aligned} \quad (3.42)$$

The resulting equivalent fringe current expressions are finite for all aspects of illumination and observation except for the case $\hat{s} = \hat{s}' = \hat{\sigma}$. In addition, there is an integrable singularity at $\hat{s} = \hat{\sigma}$ direction as expected.

3.3 Derivation of PO Equivalent Edge Currents For a Half Plane

In the following end-point evaluation

$$\vec{K}^{PO}(z) = \int_{\nu} \vec{J}_{GO}(x, z) e^{jkx\hat{x}\cdot\hat{s}} dx \quad (3.43)$$

The phase of $\vec{J}_{GO}(x, z)$ is $-kx\hat{x}\cdot\hat{s}'$. Hence, the singularity condition of the integral becomes

$$\hat{x}\cdot\hat{s} = \hat{x}\cdot\hat{s}' \quad (3.44)$$

The replacement of \hat{x} -direction by the $\hat{\sigma}$ -direction for the integration as in the case for fringe currents does not have similar effect on the PO components. Because, such a step merely replaces the cone of singular \hat{s} -directions, by another cone, defined by $\hat{s}\cdot\hat{\sigma} = \hat{s}'\cdot\hat{\sigma}$ and only for grazing incidence, $\hat{\sigma} = \hat{s}'$, does the latter collapse into a single direction, $\hat{s} = \hat{\sigma}$. However, the above argument assumes a skew coordinate direction fixed by the incidence angle for all observation directions. In fact, for equivalent currents there is no need for such a restriction, the skew coordinate direction may be determined by both the incident and observation directions (\hat{s}' and \hat{s}). So, for each observation direction, the skew coordinate direction on the surface of the half plane is determined separately.

To apply this approach, we will again use the (σ, z) skew coordinate system as shown in Figure 3.7 with an arbitrary skewness angle θ as follows

$$x = \sigma \sin \theta \quad (3.45)$$

$$z = z + \sigma \cos \theta \quad (3.46)$$

Then the following end-point contribution

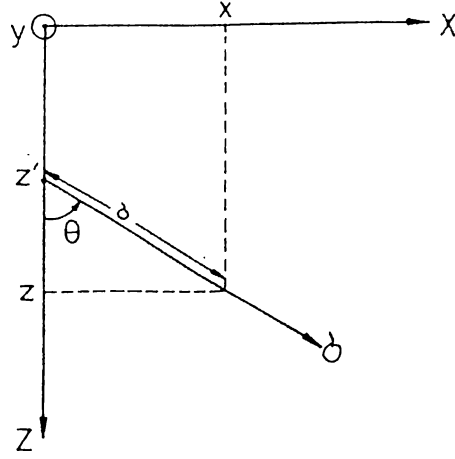


Figure 3.7: Skew Coordinate System

$$\vec{K}^{PO}(z) = \sin \theta \int_0^{\delta} \vec{J}_{GO}(\sigma \sin \theta, z + \sigma \cos \theta) e^{jk\sigma \delta \cdot \hat{s}} d\sigma \quad (3.47)$$

is evaluated as

$$K_x^{PO} = 2Y \sin \beta' - \frac{\sin \theta}{jk[(\sin \beta' \cos \phi' + \sin \beta \cos \phi) \sin \theta + \cos \theta(\cos \beta - \cos \beta')]} \quad (3.48)$$

$$K_z^{PO} = -\frac{2Y \cos \phi' \cos \beta' \sin \theta}{[(\sin \beta' \cos \phi' + \sin \beta \cos \phi) \sin \theta + \cos \theta(\cos \beta - \cos \beta')]} + \frac{2Y \sin \phi' \sin \theta}{[(\sin \beta' \cos \phi' + \sin \beta \cos \phi) \sin \theta + \cos \theta(\cos \beta - \cos \beta')]} \quad (3.49)$$

The PO equivalent edge currents are then obtained

$$\mathbf{I}^{PO} = -\frac{2Y}{jk} E_z^i \frac{\sin \phi' \sin \theta}{\sin \beta'[(\sin \beta' \cos \phi' + \sin \beta \cos \phi) \sin \theta + \cos \theta(\cos \beta - \cos \beta')]} + \frac{2}{jk} H_z^i \sin \theta \frac{\cot \beta' \cos \phi' + \cot \beta \cos \phi}{[(\sin \beta' \cos \phi' + \sin \beta \cos \phi) \sin \theta + \cos \theta(\cos \beta - \cos \beta')]} \quad (3.50)$$

$$\mathbf{M}^{PO} = \frac{2Z}{jk} H_z^i \frac{\sin \phi \sin \theta}{\sin \beta [(\sin \beta' \cos \phi' + \sin \beta \cos \phi) \sin \theta + \cos \theta (\cos \beta - \cos \beta')]} \quad (3.51)$$

It is seen that, these expressions are the function of the skewness angle θ . Hence they are nonunique.

Let

$$\mathbf{I} = \mathbf{I}^f + \mathbf{I}^{PO} \quad (3.52)$$

$$\mathbf{M} = \mathbf{M}^f + \mathbf{M}^{PO} \quad (3.53)$$

To find the radiation from the equivalent line currents \mathbf{I} and \mathbf{M} , we need to the expressions for the equivalent currents at $\beta = \beta'$ direction (See Appendix A). For that reason, it is observed that

$$\mathbf{I}^f(\beta = \beta') + \mathbf{I}^{PO}(\beta = \beta') = \mathbf{I}_{GTD} \quad (3.54)$$

$$\mathbf{M}^f(\beta = \beta') + \mathbf{M}^{PO}(\beta = \beta') = \mathbf{M}_{GTD} \quad (3.55)$$

This means that, the radiated electric field from the fringe and PO equivalent currents is independent from the arbitrary skewness angle θ and it exactly yields the GTD field.

On the other hand, the selection of θ represents the singularity map of the PO equivalent currents. At $\beta = \beta'$, the PO equivalent currents reduce to the following ones.

$$\mathbf{I}^{PO}(\beta = \beta') = \frac{2Y}{jk} E_z^i \frac{\sin \phi'}{\sin^2 \beta (\cos \phi + \cos \phi')} + \frac{2}{jk} H_z^i \frac{\cot \beta}{\sin \beta} \quad (3.56)$$

$$\mathbf{M}^{PO}(\beta = \beta') = \frac{2}{jkY} H_z^i \frac{\sin \phi}{\sin^2 \beta (\cos \phi + \cos \phi')} \quad (3.57)$$

These expressions are only singular at the incident and reflected transition regions. But the PO equivalent currents may have additional singularities depending on the selection of θ .

Accordingly, depending on both the incident and the observation directions if we choose the skewness angle θ as follows

$$\cot \theta = \frac{\cos \beta - \cos \beta'}{\sin \beta' \cos \phi' + \sin \beta \cos \phi} \quad (3.58)$$

Then PO equivalent currents become

$$\begin{aligned} \mathbf{I}^{PO} &= -\frac{2Y'}{jk} E_z^i \frac{\sin \phi' (\sin \beta \cos \phi + \sin \beta' \cos \phi')}{\sin \beta' [(\cos \beta - \cos \beta')^2 + (\sin \beta \cos \phi + \sin \beta' \cos \phi')^2]} \\ &+ \frac{2}{jk} H_z^i \frac{\sin \phi (\sin \beta \cos \phi + \sin \beta' \cos \phi')}{[(\cos \beta - \cos \beta')^2 + (\sin \beta \cos \phi + \sin \beta' \cos \phi')^2]} \end{aligned} \quad (3.59)$$

$$\mathbf{M}^{PO} = \frac{2Z}{jk} H_z^i \frac{\sin \phi (\sin \beta \cos \phi + \sin \beta' \cos \phi')}{[(\cos \beta - \cos \beta')^2 + (\sin \beta \cos \phi + \sin \beta' \cos \phi')^2]} \quad (3.60)$$

It is noted that the equivalent current expressions given in (3.59) and (3.60) are the same as the ones in [6] where they are determined for a finite size plate by an application of Stokes' theorem.

When the singularities are examined, the following conditions are obtained.

$$\phi + \phi' = \pi \quad (3.61)$$

and

$$\beta = \beta' \quad (3.62)$$

This represents the incident and reflected shadow boundaries on the Keller Cone and we see that, the singular directions are not expanded by this selection of θ .

Physically, the direction of skew coordinate $\hat{\sigma}$ in this case is the direction of the projection of $(\hat{s} - \hat{s}')$ vector onto the half-plane. It is a function of both \hat{s}' and \hat{s} , as described earlier. The natural question to ask at this point is what happens when $(\hat{s} - \hat{s}')$ vector has zero projection on the half-plane; in other

words, when $(\hat{s} - \hat{s}')$ has only normal component to the half plane surface. In this case, the above definition of $\hat{\sigma}$ fails. However, a close examination reveals that when $(\hat{s} - \hat{s}')$ vector has only normal component to the half-plane, the observation direction is either on the incident boundary ($\hat{s} = \hat{s}'$) or on the shadow boundary of the Keller Cone. Both of these cases correspond to directions for which the field is non ray-optical and the equivalent current concept is not valid.

3.4 Higher Order Equivalent Currents

When a perfectly conducting flat plate is illuminated by a plane wave, the fringe and PO equivalent currents due to the first order diffraction will be excited on the edges. The radiation from these currents yields the single edge diffracted fields. But to obtain more accurate results, it may be necessary to include the multiple diffractions between the edges. Therefore, equivalent current method can be modified to include the higher order interactions. Accordingly, the fields of the multiple diffracted rays between the plate edges are computed by constructing the corresponding equivalent edge currents and using them to compute the far scattered field. This procedure provide us to obtain the contribution of the higher order diffractions to the total far scattered field.

Consider a perfectly conducting flat plate which is illuminated by a plane wave as in Figure 3.7.

It is known that the diffracted fields from a point on the edge is given by UTD as follows

$$\begin{bmatrix} E_{\beta}^d \\ E_{\phi}^d \end{bmatrix} = - \begin{bmatrix} D_s & \mathbf{o} \\ \mathbf{o} & D_h \end{bmatrix} \begin{bmatrix} E_{\beta}^i \\ E_{\phi}^i \end{bmatrix} \quad (3.63)$$

$$D_s = - \frac{e^{-j\pi/4}}{\sqrt{2\pi k \sin \beta}} \left[\frac{\mathbf{F}[kLa(\phi - \phi')]}{\cos \frac{\phi - \phi'}{2}} + \frac{\mathbf{F}[kLa(\phi + \phi')]}{\cos \frac{\phi + \phi'}{2}} \right] \quad (3.64)$$

where

$$a(\beta) = 2 \cos^2(\beta/2) \quad (3.65)$$

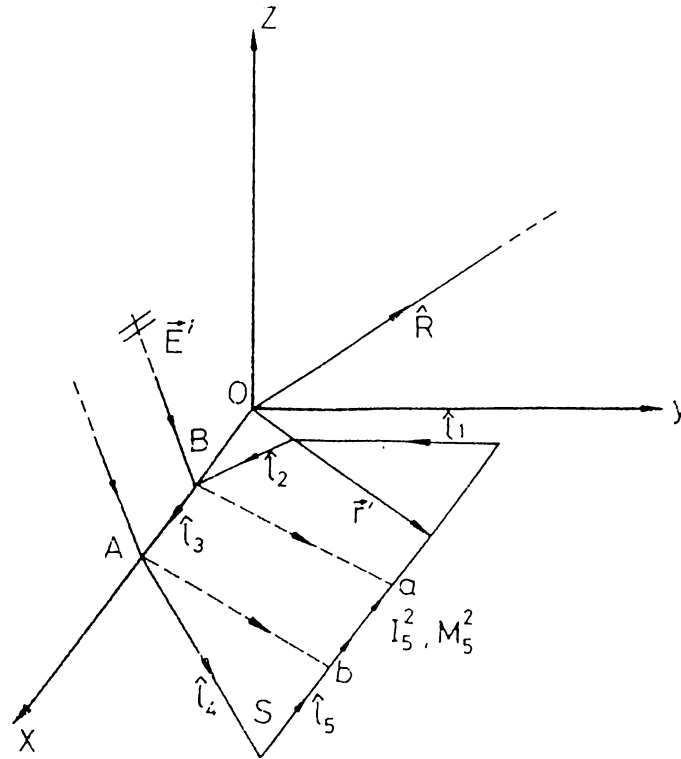


Figure 3.8: Edge interactions in a flat plate

and

$$L = \rho \sin^2 \beta \quad (3.66)$$

with the (β, ϕ) coordinate system which is defined at the diffraction point.

On the other hand, it is assumed that the diffracted field from the second edge is almost a plane wave when it illuminates the fifth edge. The diffracted rays from the edge 2 are incident to the edge 5 with the following tangential fields.

$$\begin{aligned} E_{tan}^i(\text{at edge } \bar{5}) &= \hat{l}_5 \cdot \vec{E}^d \\ &= 0 \end{aligned} \quad (3.67)$$

$$H_{tan}^i(\text{at edge } \bar{5}) = \hat{l}_5 \cdot \vec{H}^d \quad (3.68)$$

Then the equivalent edge currents at edge 5 due to double diffraction is given by

$$\mathbf{I}_5^2 = \mathbf{I}_f^2(H_{tan}^i(at\ edge 5), \beta, \beta', \phi, \phi') + \mathbf{I}_{pO}^2(H_{tan}^i(at\ edge 5), \beta, \beta', \phi, \phi') \quad (3.69)$$

$$\mathbf{M}_5^2 = \mathbf{M}_f^2(H_{tan}^i(at\ edge 5), \beta, \beta', \phi, \phi') + \mathbf{M}_{pO}^2(H_{tan}^i(at\ edge 5), \beta, \beta', \phi, \phi') \quad (3.70)$$

The radiated electric field from these equivalent currents.

$$\vec{E} = \frac{jkZ}{4\pi} \frac{e^{-jkR}}{R} \int_a^b [\hat{R} \times \hat{R} \times \vec{I}_5^2 + Y \hat{R} \times \vec{M}_5^2] e^{jk_x x} e^{jk_z z} dl \quad (3.71)$$

where \hat{R} is the observation direction and $k_x = k\hat{R} \cdot \hat{x}$, $k_y = k\hat{R} \cdot \hat{y}$. In the notation of the higher order currents I_q^m , m represents the order of the diffraction and q shows the number of the edge that equivalent currents exist.

In the analysis of higher order diffractions one has to consider the shadowing effect of the surface diffracted rays. Since this causes to the illumination regions. In the radiation integral, a and b represent the limits of the illumination region on edge 5. It is dependent to the incident wave direction, polarization and the geometry of the plate. If the similar integral is repeated for each straight part of the edge by defining the appropriate integration limits on the opposite side of the plate. Then the sum of the integration contributions will be equivalent to the second order diffraction.

Chapter 4

BACK SCATTERING FROM FLAT PLATES

In this chapter, to examine the accuracy of the fringe and PO equivalent edge currents, we applied them to the problem of backscattering from the perfectly conducting rectangular and triangular plates.

Eventhough there is no analytical solution to these plate problems, the calculations of the backscattered field has been investigated by some authors using high frequency techniques.

For the square plate problem, Ross[10] has applied the GTD and PO methods to predict the monostatic RCS. Ross also obtained a wide range of measured data[10] and his results were in agreement with the measurements except for the regions near edge-on incidence. Later, more accurate results are obtained by Sitka[9] who employed GTD based equivalent currents and included the higher order equivalent currents into the analysis. The results for the backscattering from the triangular plate are also obtained in [9].

In the present analysis, we applied the fringe and PO components of the equivalent edge currents to the same backscattering problems from the square and triangular plates. In addition, the currents are combined with UTD to include the contributions of the higher order diffractions as explained in section 3.5. The analysis is also performed for E and H polarization cases separately. For each case, the results are compared with the previous analysis of Sitka and measured data.

It is known that the fringe and PO equivalent edge currents have the infinities in the incident and reflection shadow boundaries on the Keller Cone.

Therefore, the backscattering results from the flat plates at the broadside directions become singular. On the other hand, UTD plane wave diffraction coefficients are used to consider the edge interactions. But in the transition regions, the diffracted fields from the edges are not ray optical.

The total equivalent currents are given by

$$\mathbf{I} = Y E_{tan}^i D_s(\phi', \phi, \beta', \beta) + H_{tan}^i D_2(\phi', \phi, \beta', \beta) \quad (4.1)$$

$$\mathbf{M} = Z H_{tan}^i D_h(\phi', \phi, \beta', \beta) \quad (4.2)$$

where

$$D_{s,h,2}(\phi', \phi, \beta', \beta) = d_{s,h,2}^f(\phi', \phi, \beta', \beta) + d_{s,h,2}^{PO}(\phi', \phi, \beta', \beta) \quad (4.3)$$

where $d_{s,h,2}^f$ and $d_{s,h,2}^{PO}$ expressions are due to the fringe and PO parts of the equivalent current components. It is assumed that the equivalent currents exist on the edges in the direction of the edge's tangent vector.

Two types of polarization for the incident plane wave is examined separately. E-plane polarization occurs when the direction of the incident electric field is in the observation plane. If the observation plane is the xz-plane, then the E-polarized plane wave becomes;

$$\vec{E}^i = e^{jk(x \sin \theta \cos \phi + z \cos \theta)} \hat{a}_\theta \quad (4.4)$$

$$\vec{H}^i = Y \hat{R} \times \vec{E}^i \quad (4.5)$$

Similarly, H-plane polarization occurs when the direction of the incident H field is in the observation plane.

H-polarized plane wave;

$$\vec{E}^i = e^{jk(x \sin \theta \cos \phi + z \cos \theta)} \hat{a}_\phi \quad (4.6)$$

$$\vec{H}^i = Y \hat{R} \times \vec{E}^i \quad (4.7)$$

4.1 Square Plate

Let a perfectly conducting square plate is illuminated by a plane wave with the propagating vector \hat{s}_i as shown in Figure 4.1. It is seen that xz-plane is

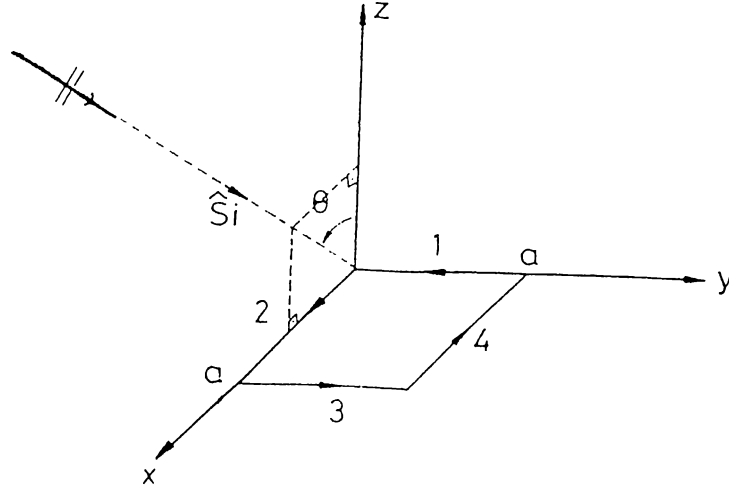


Figure 4.1: Perfectly Conducting Square Plate

the observation plane and the first order equivalent currents are excited on the edges of the square plate. The length of the plate is shown by "a".

Then the single diffracted fields from each of the edges of the square plate are evaluated by using the total equivalent edge currents as follows

From edge 1:

$$E_{\theta 1}^1 = \frac{jk}{4\pi} [D_1(\phi', \phi, \beta', \beta) H_{tan}^i] a \frac{e^{-jkr}}{r} \quad (4.8)$$

$$E_{\phi 1}^1 = \frac{jk}{4\pi} [D_s(\phi', \phi, \beta', \beta) E_{tan}^i + D_2(\phi', \phi, \beta', \beta) H_{tan}^i] a \frac{e^{-jkr}}{r} \quad (4.9)$$

where

$$\beta = \beta' = \pi/2 \quad (4.10)$$

and

$$\phi = \phi' = \pi/2 - \theta \quad (4.11)$$

From edge 2:

$$E_{\theta 2}^1 = -\frac{jk}{4\pi} [\cos \theta (D_s(\phi', \phi, \beta', \beta) E_{tan}^i + D_2(\phi', \phi, \beta', \beta) H_{tan}^i)] W(\theta, a) \frac{e^{-jkr}}{r} \quad (4.12)$$

$$E_{\phi 2}^1 = \frac{jk}{4\pi} [D_h(\phi', \phi, \beta', \beta) H_{tan}^i \cos \theta] W(\theta, a) \frac{e^{-jkr}}{r} \quad (4.13)$$

where

$$\beta' = \pi/2 + \theta \quad (4.14)$$

$$\beta = \pi/2 - \theta \quad (4.15)$$

and

$$\phi' = \phi = \pi/2 \quad (4.16)$$

From edge 3:

$$E_{\theta 3}^1 = -\frac{jk}{4\pi} [D_h(\phi', \phi, \beta', \beta) H_{tan}^i] a \frac{e^{-jkr}}{r} \quad (4.17)$$

$$E_{\phi 3}^1 = -\frac{jk}{4\pi} [D_s(\phi', \phi, \beta', \beta) E_{tan}^i + D_2(\phi', \phi, \beta', \beta) H_{tan}^i] a \frac{e^{-jkr}}{r} \quad (4.18)$$

where

$$\beta = \beta' = \pi/2 \quad (4.19)$$

and

$$\phi' = \phi = \pi/2 + \theta \quad (4.20)$$

From edge 4:

$$E_{\theta 4}^1 = \frac{jk}{4\pi} [\cos \theta (D_s(\phi', \phi, \beta', \beta) E_{tan}^i + D_2(\phi', \phi, \beta', \beta) H_{tan}^i)] W(\theta, a) \frac{e^{-jkr}}{r} \quad (4.21)$$

$$E_{\phi 4}^1 = -\frac{jk}{4\pi} [D_h(\phi', \phi, \beta', \beta) H_{tan}^i \cos \theta] W(\theta, a) \frac{e^{-jkr}}{r} \quad (4.22)$$

where

$$\beta' = \pi/2 - \theta \quad (4.23)$$

$$\beta = \pi/2 + \theta \quad (4.24)$$

and

$$\phi' = \phi = \pi/2 \quad (4.25)$$

with

$$\begin{aligned} W(\theta, a) &= \int_0^a e^{2jk \cos \theta z} dz \\ &= a e^{jk a \sin \theta} \frac{\sin(ka \sin \theta)}{ka \sin \theta} \end{aligned} \quad (4.26)$$

In the representation E_{nm}^q , m represents the edge number, n shows the electric field component and q is the single edge diffraction. Then the total single diffracted field becomes

$$\vec{E}^1 = E_\theta^1 \vec{a}_\theta + E_\phi^1 \vec{a}_\phi \quad (4.27)$$

where

θ component:

$$E_\theta^1 = E_{\theta 1}^1 + E_{\theta 2}^1 + E_{\theta 3}^1 + E_{\theta 4}^1 \quad (4.28)$$

ϕ component:

$$E_\phi^1 = E_{\phi 1}^1 + E_{\phi 2}^1 + E_{\phi 3}^1 + E_{\phi 4}^1 \quad (4.29)$$

The higher order diffraction mechanisms are analyzed for E and H plane cases in the next sections.

4.1.1 E-Polarization

When the higher order interactions between the edges of the square plate are considered according to UTD, then it is observed that the edges 2 and 4 don't cause diffracted rays on the surface. However, the opposite edges 1 and 3 interact correspondingly. Therefore, due to the double diffraction, the following second order edge currents exist on edge 3.

$$\mathbf{I}_3^2 = H_{tan}^i D_2(\phi' = 0, \phi = \pi/2 + \theta, \beta = \beta' = \pi/2) \quad (4.30)$$

$$\mathbf{M}_3^2 = Z H_{tan}^i D_h(\phi' = 0, \phi = \pi/2 + \theta, \beta = \beta' = \pi/2) \quad (4.31)$$

where

$$H_{tan}^i = -\frac{1}{2} H^i(\text{at edge 1}) D_{\mathbf{h}}^1(\phi' = \pi/2 - \theta, \phi = 0, \beta = \pi/2, a) \frac{e^{-jka}}{\sqrt{a}} \quad (4.32)$$

where $D_{\mathbf{h}}^1$ is the UTD hard diffraction coefficient on edge 1 and the factor 1/2 is due to grazing incidence. The second order currents \vec{I}_1^2 and \vec{M}_1^2 on edge 1 can be found similarly. Then the total second order diffracted field is given by the following integral.

$$\begin{aligned} \vec{E}^2 &= \frac{jkZ}{4\pi} \frac{e^{-jkR}}{R} \left(\int_0^a [\hat{R} \times \hat{R} \times \vec{I}_1^2 + Y \hat{R} \times \vec{M}_1^2] e^{jk_y y} dy \right. \\ &\quad \left. + \int_0^a [\hat{R} \times \hat{R} \times \vec{I}_3^2 + Y \hat{R} \times \vec{M}_3^2] e^{j(k_x a + k_y y)} dy \right) \quad (4.33) \end{aligned}$$

The third order diffractions are also computed by using the similar approach.

4.1.2 H-polarization

In H-polarization case, only the edges 2 and 4 cause diffracted rays on the surface. In the analysis of the higher order diffraction mechanisms, it is observed that the diffracted rays from the edge 2 illuminate the whole of the edge 1 and a part of the edge 4 for $\theta < \pi/4$. On the other hand, for $\theta > \pi/4$ only edge 1 is partially illuminated by the diffracted rays from the edge 2 as shown in Figure 4.2.

Then the second order equivalent currents on the edges 1 and 4, due to the double diffraction, are given by

On Edge 1:

$$\mathbf{I}_1^2 = H_{tan}^i D_2(\phi' = 0, \phi = \pi/2 - \theta, \beta' = \pi - \theta, \beta = \pi/2) \quad (4.34)$$

$$\mathbf{M}_1^2 = Z H_{tan}^i D_{\mathbf{h}}(\phi' = 0, \phi = \pi/2 - \theta, \beta' = \pi - \theta, \beta = \pi/2) \quad (4.35)$$

where

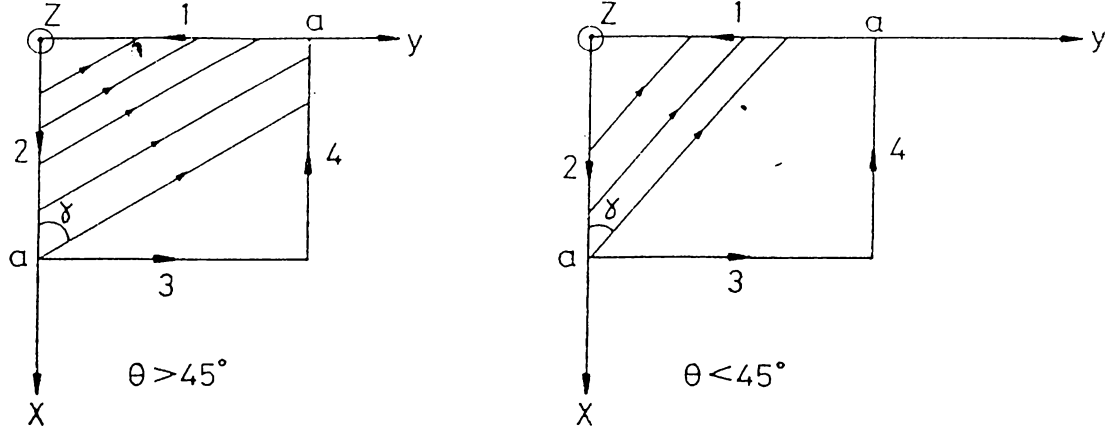


Figure 4.2: Edge Interactions in the Square Plate

$$H_{tan}^i = \frac{1}{2} H^i(\text{at edge 2}) \sin \theta D_h^2(\phi' = \pi/2, \phi = 0, \beta = \pi/2 + \theta, s) \frac{e^{-jks}}{\sqrt{s}} \quad (4.36)$$

with

$$s = \frac{y}{\cos \theta} \quad (4.37)$$

On Edge 4:

$$I_4^2 = H_{tan}^i D_2(\phi' = 0, \phi = \pi/2, \beta' = \pi/2 - \theta, \beta = \pi/2 + \theta) \quad (4.38)$$

$$M_4^2 = Z H_{tan}^i D_h(\phi' = 0, \phi = \pi/2, \beta' = \pi/2 - \theta, \beta = \pi/2 + \theta) \quad (4.39)$$

where

$$H_{tan}^i = \frac{1}{2} H^i(\text{at edge 2}) \cos \theta D_h^4(\phi' = \pi/2, \phi = 0, \beta = \pi/2 + \theta, s) \frac{e^{-jks}}{\sqrt{s}} \quad (4.40)$$

with

$$s = \frac{a}{\cos \theta} \quad (4.41)$$

Then the contribution of the second edge to the total second order diffraction is given by

$$\begin{aligned} \vec{E}_2^2 &= \frac{jkZ}{4\pi} \frac{e^{-jkR}}{R} \left(\int_0^{y_{max}} [\hat{R} \times \hat{R} \times \vec{I}_1^2 + Y \hat{R} \times \vec{M}_1^2] e^{jk_y y} dy \right. \\ &\quad \left. + \int_0^{x_{max}} [\hat{R} \times \hat{R} \times \vec{I}_4^2 + Y \hat{R} \times \vec{M}_4^2] e^{j(k_x a + k_y y)} dx \right) \end{aligned} \quad (4.42)$$

where

$$y_{max} = \begin{cases} a & \theta < \pi/4 \\ a \cot \theta & \theta > \pi/4 \end{cases} \quad (4.43)$$

and

$$x_{max} = \begin{cases} a(1 - \tan \theta) & \theta < \pi/4 \\ 0 & \theta > \pi/4 \end{cases} \quad (4.44)$$

The contribution of the edge 4 to the second order diffraction is computed in a similar way. Then the total second order diffracted field is evaluated as

$$\vec{E}^2 = \vec{E}_2^2 + \vec{E}_4^2 \quad (4.45)$$

4.2 Triangular Plate

The perfectly conducting triangular plate, as shown in Figure 4.3, is illuminated by a plane wave which lies in the xz -plane. The xz -plane is again the observation plane.

The single diffracted fields from the edges of the triangular plate are obtained as follows

From edge 1:

$$E_{\theta 1}^1 = -\frac{jk}{4\pi} D_h(\phi', \phi, \beta', \beta) H_{tan}^i N(b) \quad (4.46)$$

$$E_{\phi 1}^1 = -\frac{jk}{4\pi} [D_s(\phi', \phi, \beta', \beta) E_{tan}^i + D_2(\phi', \phi, \beta', \beta) H_{tan}^i] N(b) \quad (4.47)$$

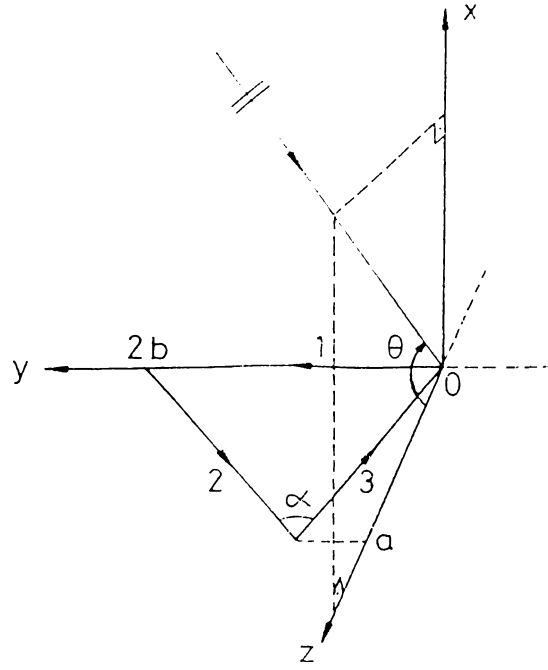


Figure 4.3: Perfectly Conducting Triangular Plate

where

$$\phi = \phi' = \theta \quad (4.48)$$

$$\beta = \beta' = \pi/2 \quad (4.49)$$

From edge 2:

$$\begin{aligned} E_{\theta 2}^1 &= \frac{jk}{4\pi} [(\sin \alpha/2 D_h(\phi', \phi, \beta', \beta) + \cos \alpha/2 \sin \theta D_2(\phi', \phi, \beta', \beta)) H_{tan}^i \\ &+ \cos \alpha/2 \sin \theta D_s(\phi', \phi, \beta', \beta) E_{tan}^i] M(\theta, a) \end{aligned} \quad (4.50)$$

$$\begin{aligned} E_{\phi 2}^1 &= \frac{jk}{4\pi} [(-\cos \alpha/2 \sin \theta D_h(\phi', \phi, \beta', \beta) + \sin \alpha/2 D_2(\phi', \phi, \beta', \beta)) H_{tan}^i \\ &+ \sin \alpha/2 D_s(\phi', \phi, \beta', \beta) E_{tan}^i] M(\theta, a) \end{aligned} \quad (4.51)$$

where

$$\beta' = \cos^{-1}(-\cos \alpha/2 \cos \theta) \quad (4.52)$$

$$\beta_o = \beta = \cos^{-1}(\cos \alpha/2 \cos \theta) \quad (4.53)$$

$$\phi' = \phi = \cos^{-1} \left[\frac{-\sin \alpha/2 \cos \theta}{\sqrt{1 - \cos^2 \theta \cos^2 \alpha/2}} \right] \quad (4.54)$$

From edge 3:

$$\begin{aligned} E_{\theta 3}^1 &= \frac{jk}{4\pi} [(-\cos \alpha/2 \sin \theta D_2(\phi', \phi, \beta', \beta) + \sin \alpha/2 D_{11}(\phi', \phi, \beta', \beta)) H_{tan}^i \\ &- \cos \alpha/2 \sin \theta D_s(\phi', \phi, \beta', \beta) E_{tan}^i] M(\theta, a) \end{aligned} \quad (4.55)$$

$$\begin{aligned} E_{\phi 3}^1 &= \frac{jk}{4\pi} [(\sin \alpha/2 D_2(\phi', \phi, \beta', \beta) + \cos \alpha/2 \sin \theta D_{11}(\phi', \phi, \beta', \beta)) H_{tan}^i \\ &+ \sin \alpha/2 D_s(\phi', \phi, \beta', \beta) E_{tan}^i] M(\theta, a) \end{aligned} \quad (4.56)$$

where

$$\beta' = \cos^{-1}(\cos \alpha/2 \cos \theta) \quad (4.57)$$

and

$$\beta = \cos^{-1}(-\cos \alpha/2 \cos \theta) \quad (4.58)$$

ϕ, ϕ' are the same as the second edge.

In addition,

$$N(b) = \int_0^{2b} dy = 2b \quad (4.59)$$

$$\begin{aligned} M(\theta, a) &= \int_0^a e^{2jk \cos \theta z} dz \\ &= a \frac{\sin(k \cos \theta a)}{k \cos \theta a} e^{jk \cos \theta a} \end{aligned} \quad (4.60)$$

The total single diffracted field becomes

$$\vec{E}^1 = E_{\theta}^1 \vec{a}_{\theta} + E_{\phi}^1 \vec{a}_{\phi} \quad (4.61)$$

where

θ component;

$$E_{\theta}^1 = E_{\theta 1}^1 + E_{\theta 2}^1 + E_{\theta 3}^1 \quad (4.62)$$

ϕ component;

$$E_{\phi}^1 = E_{\phi 1}^1 + E_{\phi 2}^1 + E_{\phi 3}^1 \quad (4.63)$$

The higher order diffraction mechanisms are analyzed for E and H polarization cases separately in the next sections.

4.2.1 E-Polarization

In this polarization, it is seen that all edges cause diffracted rays on the surface and the higher order diffraction mechanisms can be mainly split into the following two parts.

i) The diffracted rays caused by the first edge of the triangular plate illuminate the second and third edges. Then the corresponding second order equivalent edge currents on the edges 2 and 3 are given by

On edge 2:

$$\mathbf{I}_2^2 = H_{tan}^i D_2(\phi' = O, \phi, \beta' = \alpha/2, \beta) \quad (4.64)$$

$$\mathbf{M}_2^2 = Z H_{tan}^i D_h(\phi' = O, \phi, \beta' = \alpha/2, \beta) \quad (4.65)$$

where

$$H_{tan}^i = \frac{1}{2} H^i(at\ edge 1) \sin \alpha/2 D_h^1(\phi' = \theta, \phi = O, \beta = \pi/2, z) \frac{e^{-jkz}}{\sqrt{z}} \quad (4.66)$$

On edge 3:

$$\mathbf{I}_3^2 = H_{tan}^i D_2(\phi' = O, \phi, \beta' = \pi - \alpha/2, \beta) \quad (4.67)$$

$$\mathbf{M}_3^2 = Z H_{tan}^i D_h(\phi' = O, \phi, \beta' = \pi - \alpha/2, \beta) \quad (4.68)$$

where

$$H_{tan}^i = \frac{1}{2} H^i(\text{at edge1}) \sin \alpha/2 D_h^1(\phi' = \theta, \phi = O, \beta = \pi/2, z) \frac{e^{-jkz}}{\sqrt{z}} \quad (4.69)$$

ϕ is determined by equation (4.51) for each edge and β is evaluated by equations (4.53) and (4.58) for second and third edges respectively.

Then the radiation of these equivalent currents is given by

$$\begin{aligned} \vec{E}_1^2 &= \frac{jkZ}{4\pi} \frac{e^{-jkR}}{R} \left(\int_0^a [\hat{R} \times \hat{R} \times \vec{I}_2^2 + Y \hat{R} \times \vec{M}_2^2] e^{jkz \cos \theta} dz \right. \\ &\quad \left. + \int_0^a [\hat{R} \times \hat{R} \times \vec{I}_3^2 + Y \hat{R} \times \vec{M}_3^2] e^{jkz \cos \theta} dz \right) \end{aligned} \quad (4.70)$$

ii) On the other hand, we see that the diffracted rays from the edge 3 illuminate the edges 1 and 2 depending on β_o as shown in Figure 4.4.

The second order equivalent edge currents on the edges 1 and 2 due to the diffracted rays from edge 3 are given as follows

On Edge 1:

$$\mathbf{I}_1^2 = H_{tan}^i D_2(\phi' = O, \phi = \theta, \beta' = \pi/2 - \beta_o + \alpha/2, \beta = \pi/2) \quad (4.71)$$

$$\mathbf{M}_1^2 = Z H_{tan}^i D_h(\phi' = O, \phi = \theta, \beta' = \pi/2 - \beta_o + \alpha/2, \beta = \pi/2) \quad (4.72)$$

where

$$H_{tan}^i = -\frac{1}{2} H_\phi^i(\text{at edge3}) \cos(\beta_o - \alpha/2) D_h^3(\phi', \phi = O, \beta, s) \frac{e^{-jks}}{\sqrt{s}} \quad (4.73)$$

On Edge 2:

$$\mathbf{I}_2^2 = H_{tan}^i D_2(\phi' = O, \phi, \beta' = \pi - \beta_o + \alpha, \beta) \quad (4.74)$$

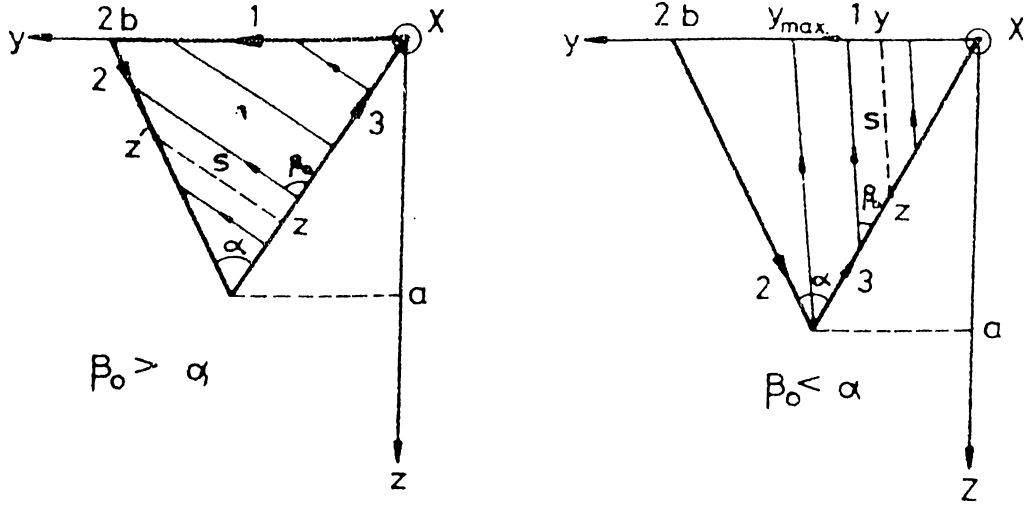


Figure 4.4: Edge interactions in the triangular plate

$$M_2^2 = Z H_{tan}^i D_b(\phi' = 0, \phi, \beta' = \pi - \beta_0 + \alpha, \beta) \quad (4.75)$$

where

$$H_{tan}^i = -\frac{1}{2} H_{\phi}^i(\text{at edge 3}) \sin(\beta_0 - \alpha) D_h^3(\phi', \phi = 0, \beta_0, s) \frac{e^{-jks}}{\sqrt{s}} \quad (4.76)$$

and

$$H_{\phi}^i(\text{at edge 3}) = Y e^{jkz \cos \theta} \quad (4.77)$$

β and ϕ for second edge are given in terms of θ with the equations (4.53) and (4.54).

In addition, s and z are the integration parameters which have the following relationships.

For Edge 1:

$$s = \frac{y}{\cos(\beta_0 - \alpha/2) \tan \alpha/2 + \sin(\beta_0 - \alpha/2)} \quad (4.78)$$

$$z = s(y) \cos(\beta_0 - \alpha/2) \quad (4.79)$$

For Edge 2:

$$\gamma = \pi/2 + \alpha/2 - \beta_o \quad (4.80)$$

$$s = 2 \tan(\alpha/2) \frac{a - z'}{\cos \gamma + \tan \alpha/2 \sin \gamma} \quad (4.81)$$

$$z = \frac{z'(\cos \gamma - \tan \alpha/2 \sin \gamma) + 2a \tan \alpha/2 \sin \gamma}{\cos \gamma + \tan \alpha/2 \sin \gamma} \quad (4.82)$$

These integration variables as shown in Figure 4.4 are substituted into the following radiation integral with the defined equivalent currents.

$$\begin{aligned} \vec{E}_3^2 &= \frac{jkZ}{4\pi} \frac{e^{-jkR}}{R} \left(\int_0^{y_{max}} [\hat{R} \times \hat{R} \times \vec{I}_1^2 + Y \hat{R} \times \vec{M}_1^2] dy \right. \\ &\quad \left. + \int_{z_{min}}^a [\hat{R} \times \hat{R} \times \vec{I}_2^2 + Y \hat{R} \times \vec{M}_2^2] e^{jkz' \cos \theta} dz' \right) \end{aligned} \quad (4.83)$$

where

$$y_{max} = \begin{cases} a[\tan \alpha/2 + \tan(\beta_o - \alpha/2)] & \beta_o < \alpha \\ a & \beta_o > \alpha \end{cases} \quad (4.84)$$

and

$$z_{min} = \begin{cases} a & \beta_o < \alpha \\ 0 & \pi/2 + \alpha/2 > \beta_o > \alpha \\ -\frac{2a \tan \alpha/2 \sin \gamma}{\cos \gamma - \tan \alpha/2 \sin \gamma} & \beta_o > \pi/2 + \alpha/2 \end{cases} \quad (4.85)$$

This procedure is repeated for the diffracted rays from edge 2. Then the following sum of all integral contributions gives the total second order diffracted field.

$$\vec{E}^2 = \vec{E}_1^2 + \vec{E}_2^2 + \vec{E}_3^2 \quad (4.86)$$

4.2.2 H-Polarization

In contrast to the E-polarization case, in H-polarization the first edge doesn't cause to the surface diffraction. However, second and third edges create the diffracted rays and the corresponding equivalent currents on the opposite edges. Therefore, the second diffraction can be computed by using the second mechanism mentioned in the previous section.

Chapter 5

COMPARISON OF THE RESULTS

Here, the results of the present analysis of the square and triangular plates will be presented and compared with the previous results of Sitka[9], Ross[10] and the measured data[9].

In both flat plates, for each polarization case, the total far scattered field is obtained by the summation of all integral contributions including computed higher order diffractions. The integrals are evaluated numerically using pulse functions with 0.01 wavelength steps. Then the total far scattered field is found as

$$\vec{E} = \vec{E}^1 + \vec{E}^2 + \vec{E}^3 \quad (5.1)$$

In the analysis, except the E-polarization for square plate, only the first and second order diffractions are used. The scattered field is observed in the backscattered direction and monostatic RCS is obtained as a function of θ .

In the backscattering from the square plate, E-plane pattern results are shown in Figure 5.1. The first, second and third order diffractions are used in the analysis. It is observed that there is no difference between our result and Sitka's solution and both of them are close to the experimental data for $\theta < 80$.

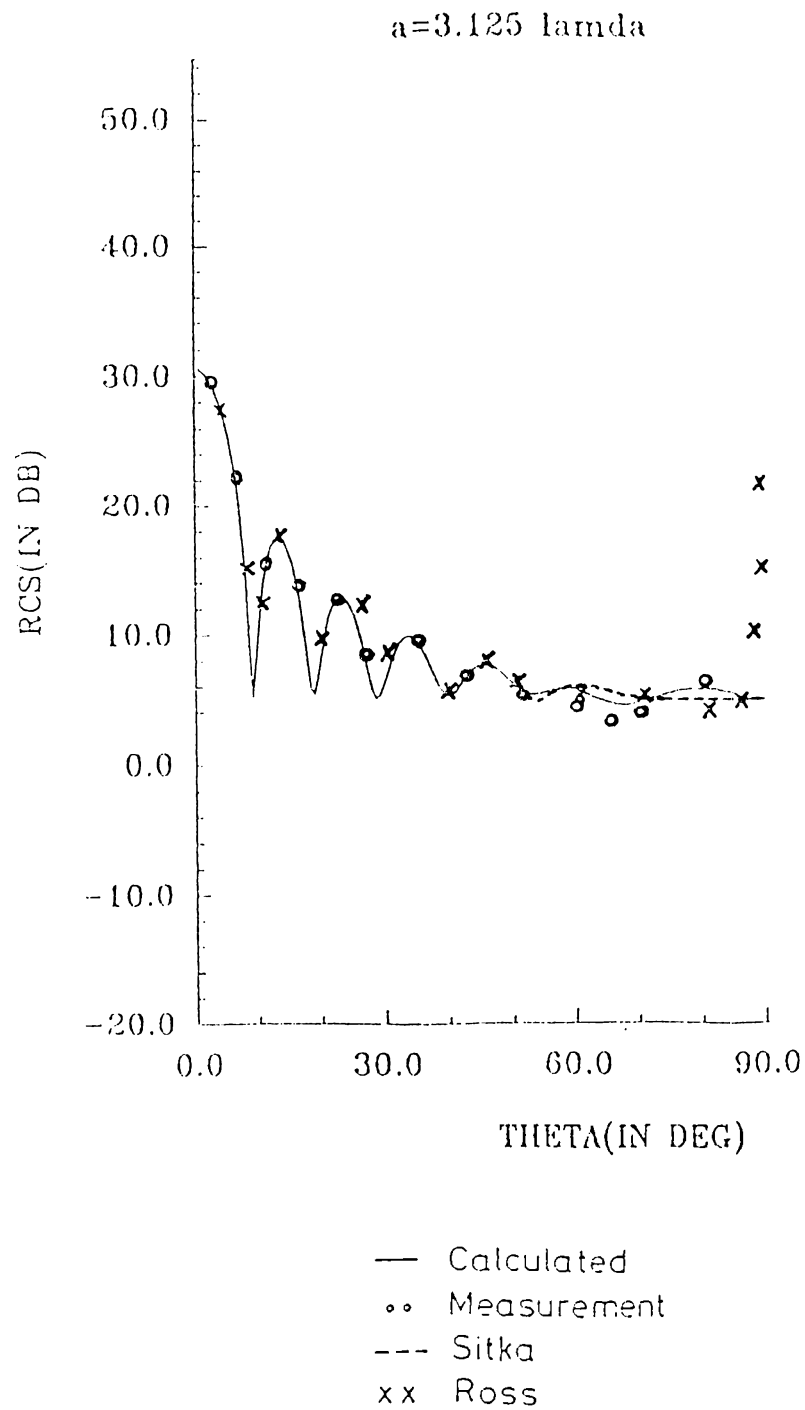
In H polarization illumination for the square plate problem, the agreement between our result and the result in [9] is good and they coincide with the experimental result away from the grazing incidence region (See Figure 5.2). Furthermore, we were able to predict the small oscillations near edge-on region by including the second order currents into the analysis.

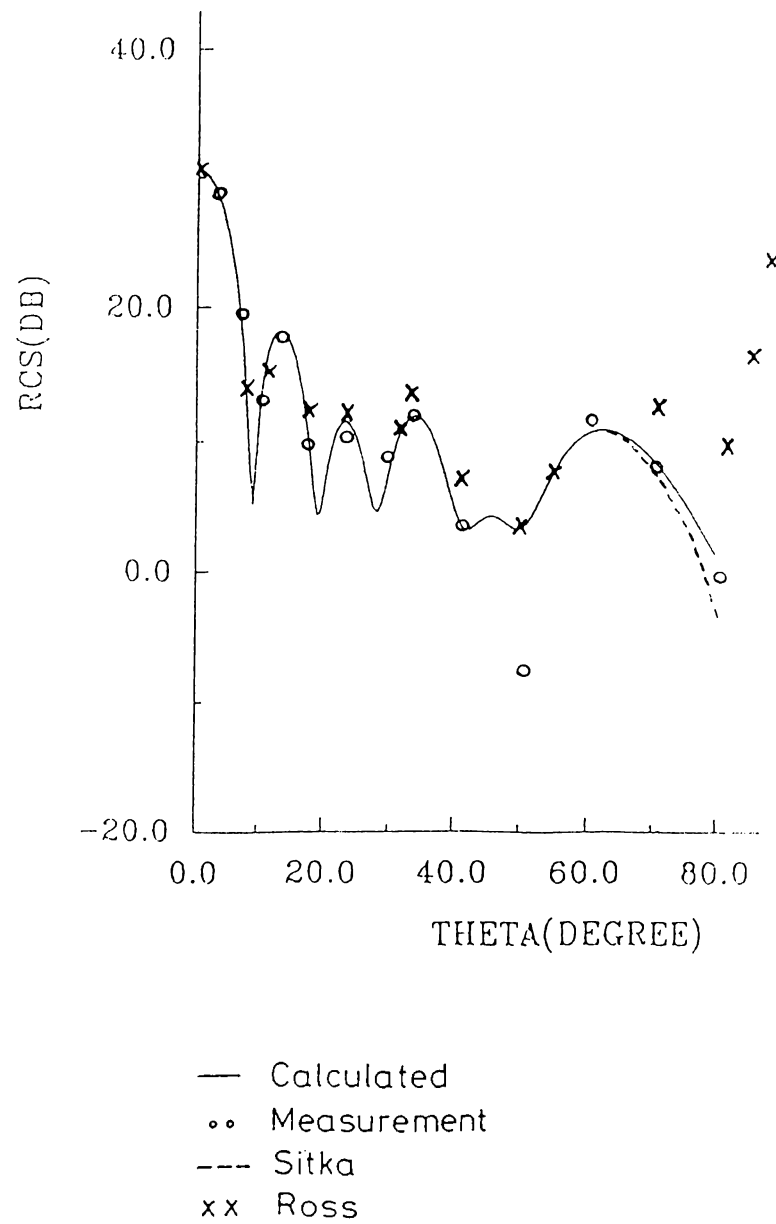
In the determination of the backscattering from the triangular plate, for

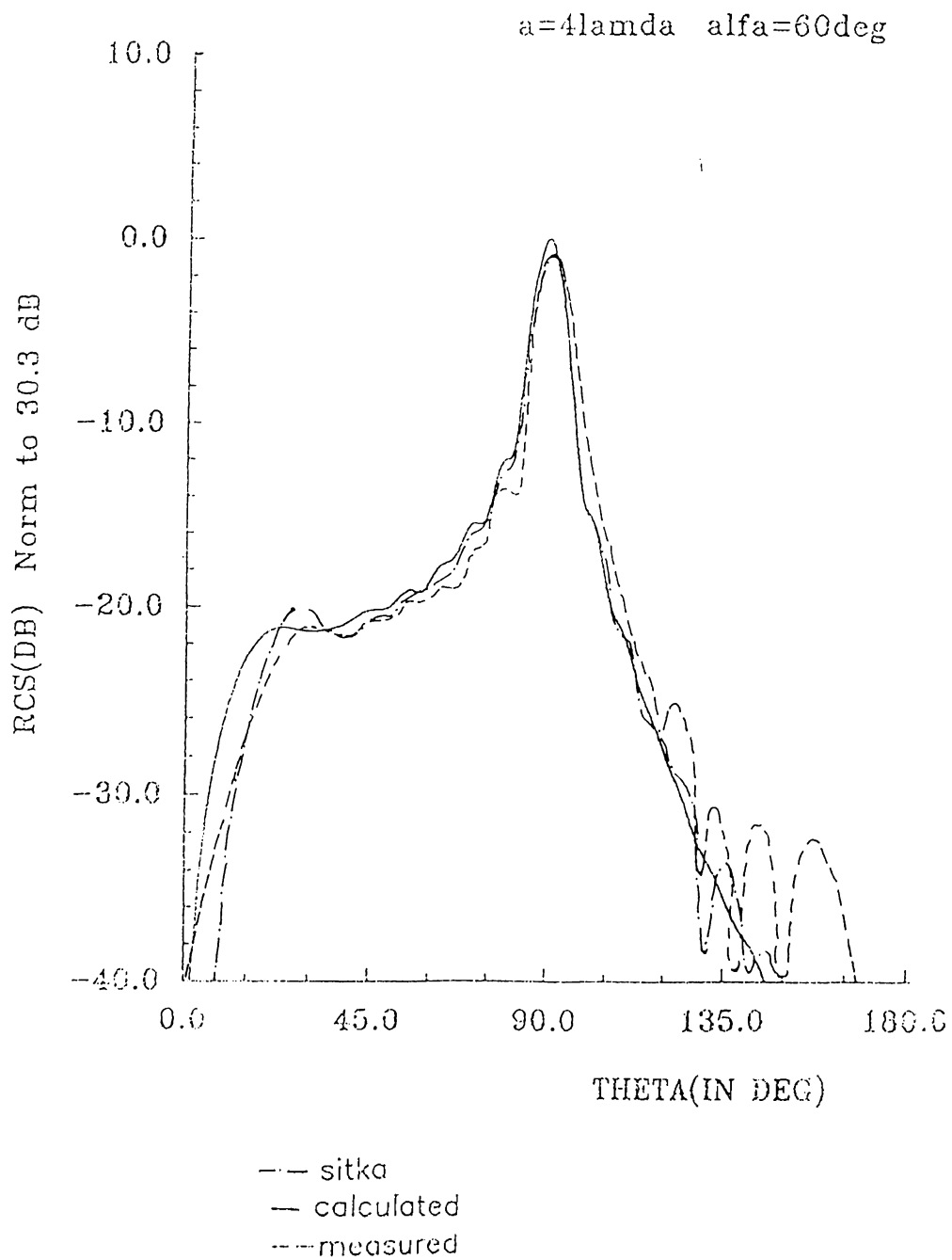
E-polarization case, only the first and second order diffractions are used in the analysis. However, in [9], Sitka has used the first, second and third order diffractions including the all edge interactions. On the other hand, in H-polarization case, although the first and third order diffractions, corner diffraction and edge wave mechanism are included to the analysis, second order diffractions are omitted by claiming that the double diffracted rays between the edges 1 and 2 of the triangle are cancelled by the diffracted rays between edges 2 and 3 in [9]. This cancellation does not occur for the new fringe and PO equivalent currents. Therefore, we used the first and second order diffractions for that polarization.

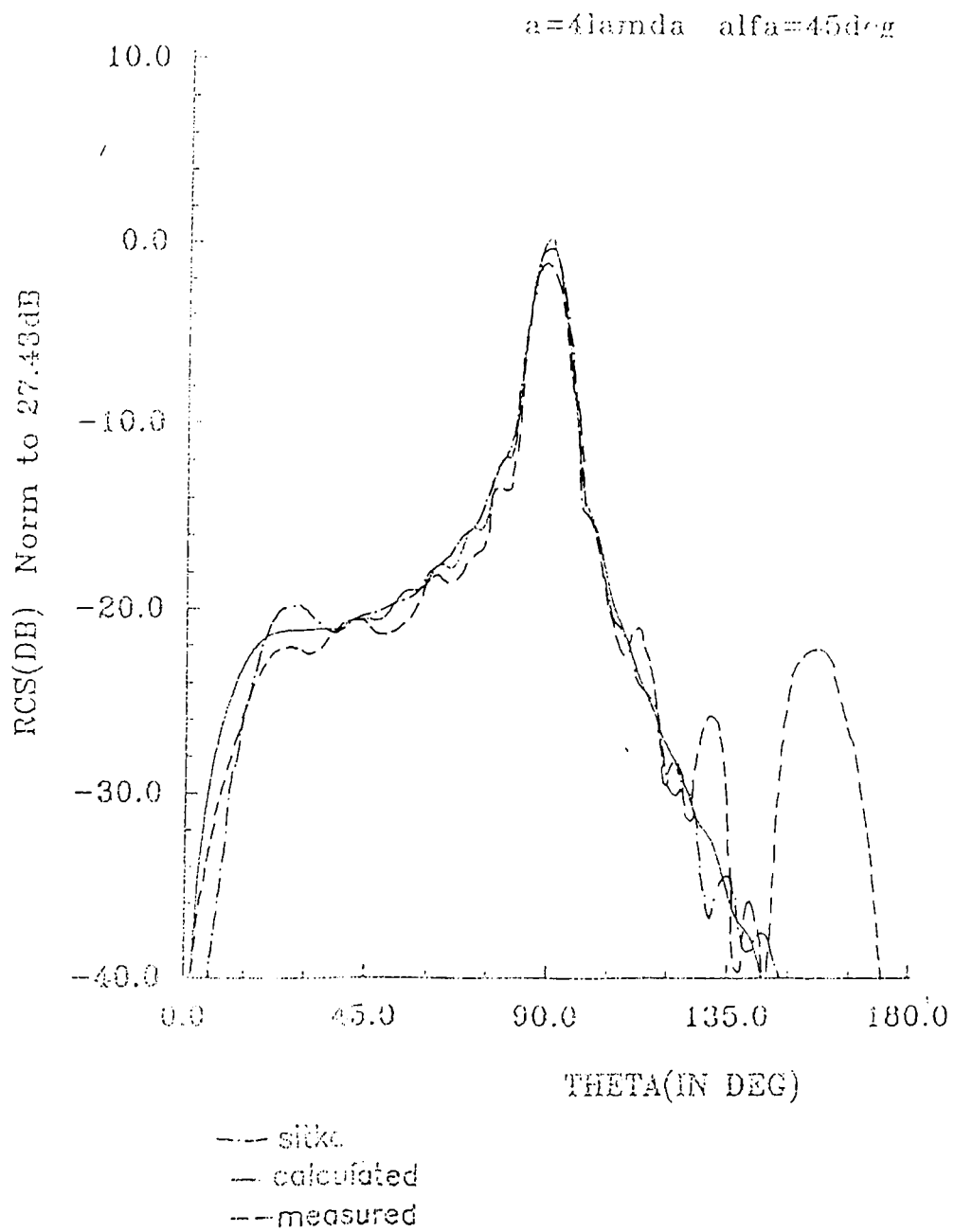
E-polarization results for the different sized triangular plates are shown in Figures 5.3-5.6. It is observed from the figures that the present solutions are closer than the ones in [9] to the measured data for $\theta < 20$. In addition, in Figure 5.5, Sitka predicts a nonzero scattered field at $\theta = 180$. However, in this analysis a zero field is obtained as expected.

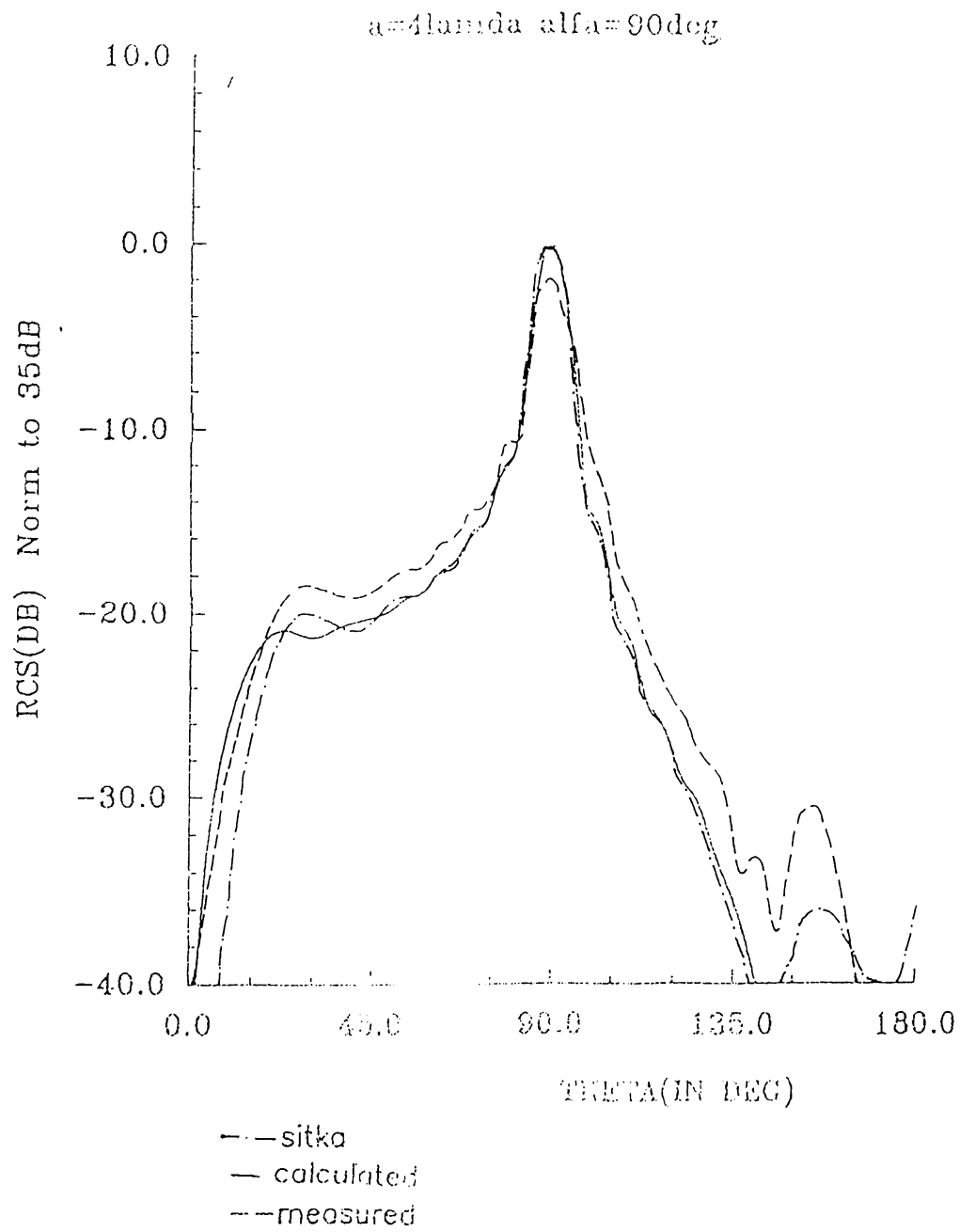
The H-plane calculations for the triangular plates are shown in Figures 5.7 and 5.8. Both present and Sitka's results are fairly accurate around the broadside direction ($45 < \theta < 120$), and our results have a slightly better prediction of the variation of the pattern for $\theta > 90$. Both results deviate from the experiments for $\theta < 45$.

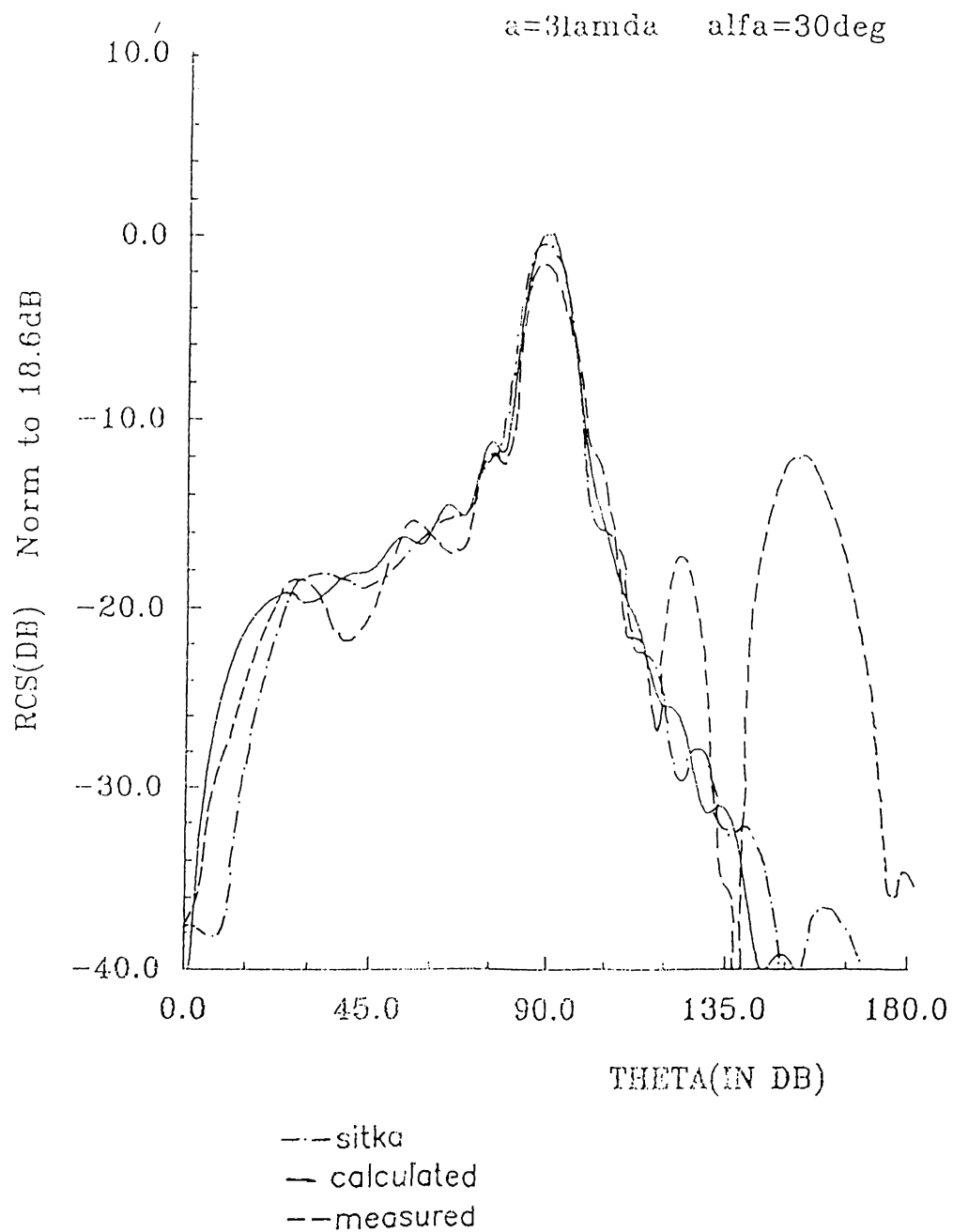
Figure 5.2: Backscattering from the square plate: H-pol ($a=3.125\lambda$)

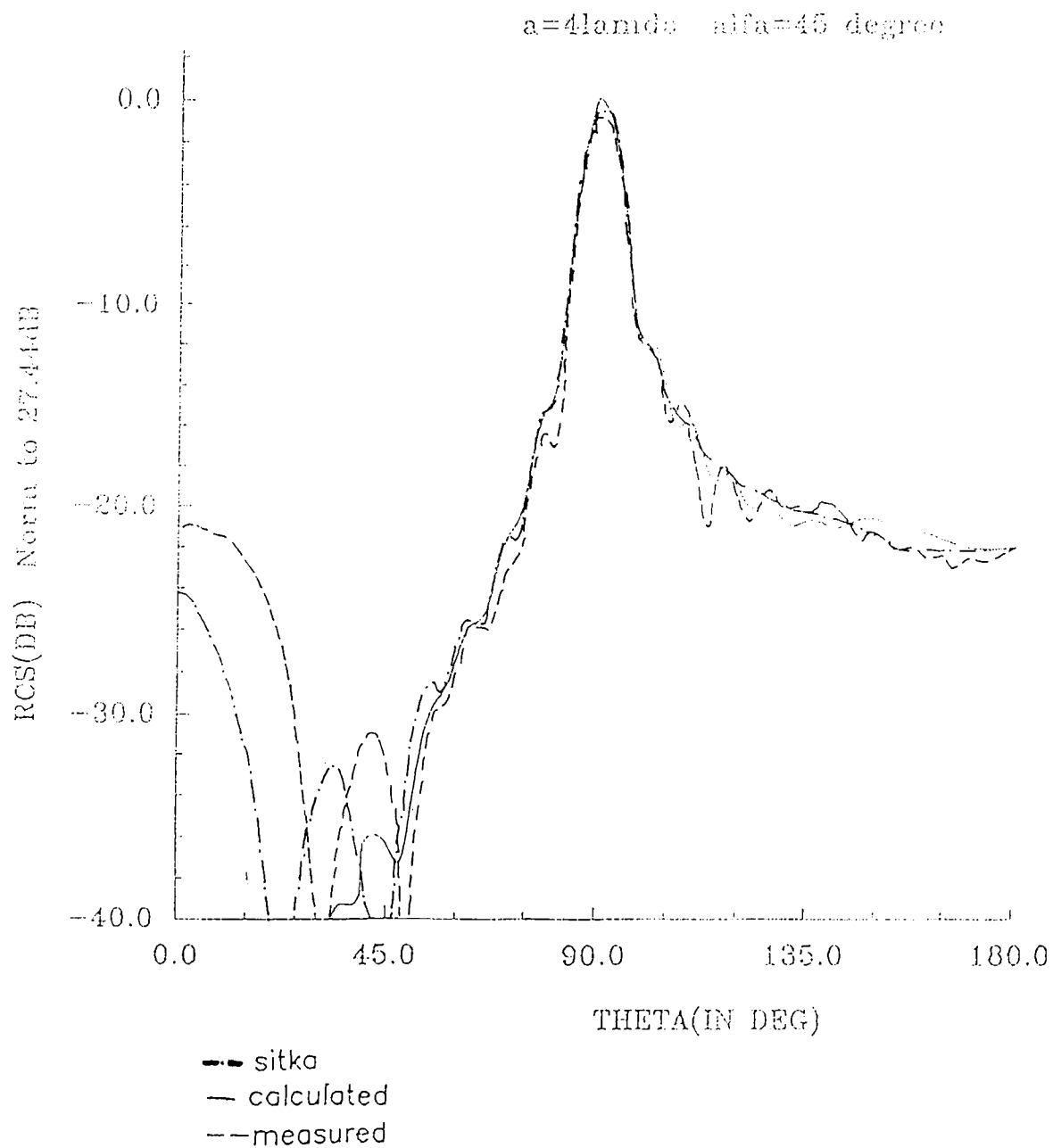
Figure 5.2: Backscattering from the square plate: Ξ -pol ($a=3.125\lambda$)

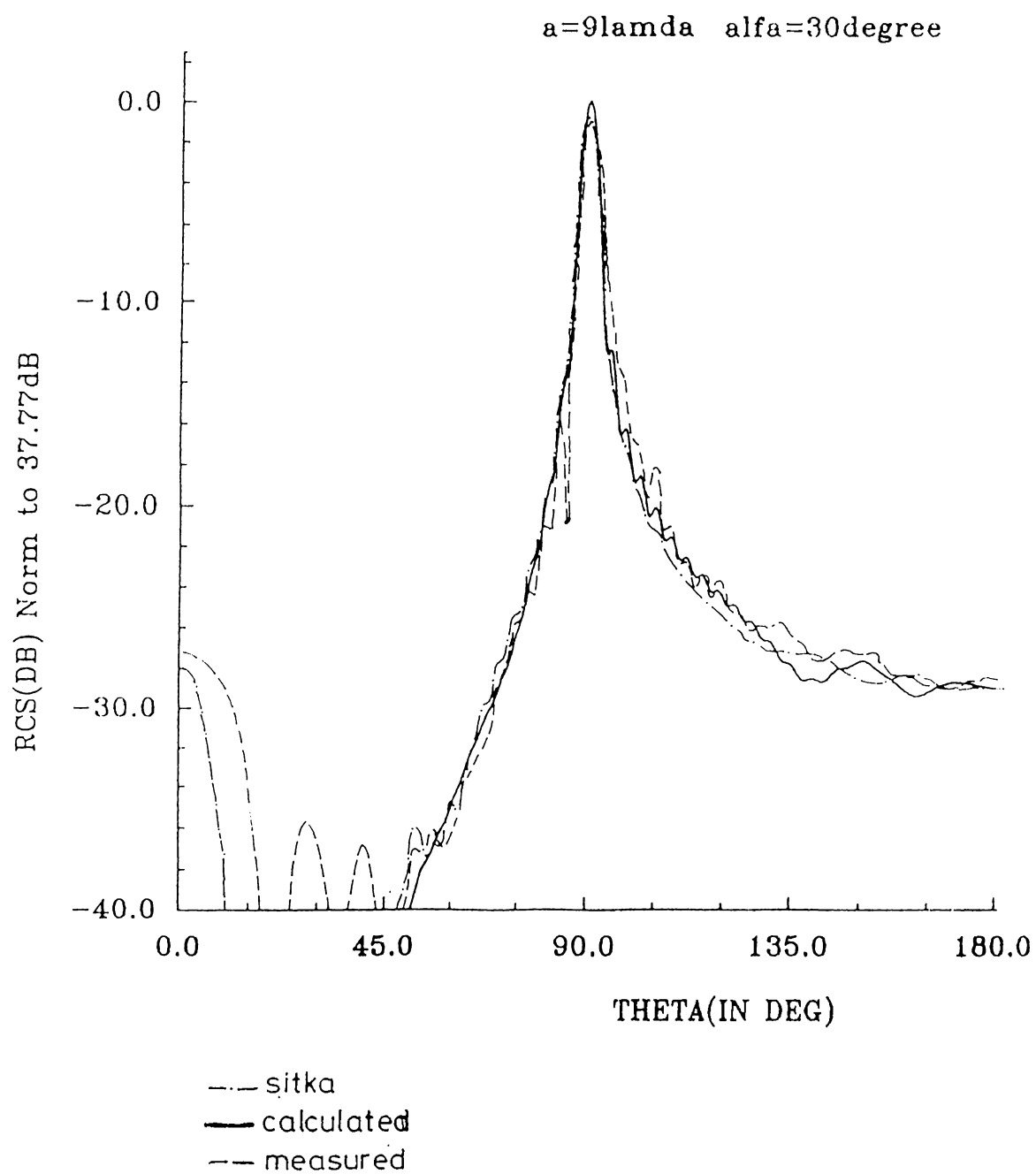
Figure 5.3: Backscattering from triangular plate: E-pol($a=4\lambda$, $\alpha=60\text{deg}$)

Figure 5.4: Backscattering from triangular plate: E-pol($a=4\lambda$, $\alpha=45\text{deg}$)

Figure 5.5: Backscattering from triangular plate: E-pol($a=4\lambda$, $\alpha=90\text{deg}$)

Figure 5.6: Backscattering from triangular plate: E-pol($a=3\lambda$, $\alpha=30\text{deg}$)

Figure 5.7: Backscattering from triangular plate: H-pol($a=4\lambda$, $\alpha=45$ deg)

Figure 5.8: Backscattering from triangular plate: H-pol($a=9\lambda$, $\alpha=30\text{deg}$)

Chapter 6

CONCLUSIONS

In the present study, we derived the PO components of the equivalent edge currents for a half plane similar to the Michaeli's approach for the elimination of the infinities of the fringe current component. By using a different selection of the skew coordinate over the half plane, we obtained the PO equivalent current expressions. It is seen that these expressions are the same with the ones obtained in [6].

Furthermore, by obtaining the PO equivalent currents depending on an arbitrary skewness angle, it is shown that the radiation from the fringe and these arbitrary PO equivalent currents are unique and yields the GTD field. Therefore, this proves the expectations that the nonunique equivalent currents must give the unique radiation.

Later, the fringe and PO equivalent currents, that is more general than the GTD based ones, are applied to the problems of the backscattering from the perfectly conducting square and triangular plates. The higher order diffractions are considered in the analysis in order to evaluate the interactions between the edges of the plates by using the UTD. Then, in the comparison of the present results with the previous results of Sitka some improvements are obtained.

Appendix A

Radiation From The Infinite Line Sources

Let an infinite line source, carrying electric and magnetic type currents I and M .

The radiated electric field from the line sources is given by

$$\vec{E} = \frac{jkZ}{4\pi} \int_{-\infty}^{\infty} [\hat{s} \times \hat{s} \times \vec{I}(z') + Y \hat{s} \times \vec{M}(z')] \frac{e^{-jk\sqrt{(z-z')^2 + \rho^2}}}{\sqrt{(z-z')^2 + \rho^2}} dz' \quad (\text{A.1})$$

where z and ρ are the observation point coordinates as shown in the following Figure.

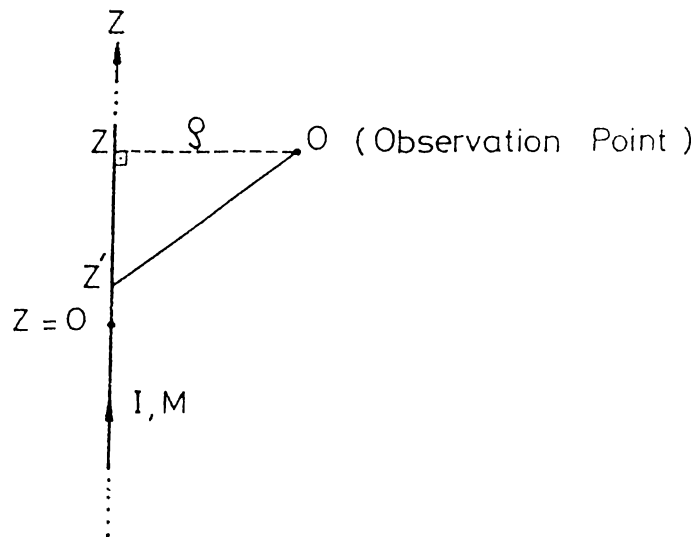


Figure A.1: Infinite line sources

If equivalent currents are in the form

$$\mathbf{I}(z') = I(z')e^{-jkz' \cos \beta'} \quad (\text{A.2})$$

$$\mathbf{M}(z') = M(z')e^{-jkz' \cos \beta'} \quad (\text{A.3})$$

Then integral becomes

$$\vec{E} = \frac{jkZ}{4\pi} \int_{-\infty}^{\infty} [\hat{s} \times \hat{s} \times \vec{I}(z') + Y \hat{s} \times \vec{M}(z')] \frac{e^{-jk(z' \cos \beta' + \sqrt{(z-z')^2 + \rho^2})}}{\sqrt{(z-z')^2 + \rho^2}} dz' \quad (\text{A.4})$$

This integral can be evaluated by the method of stationary phase. Assuming that $I(z')$ and $M(z')$ are slowly varying and k is large.

Then the phase of the integrand

$$\psi(z') = -[z' \cos \beta' + \sqrt{(z-z')^2 + \rho^2}] \quad (\text{A.5})$$

Solving $\psi'(z'_s) = 0$, the stationary point is found as $\beta = \beta'$

That is

$$\cos \beta' = \frac{z - z'}{\sqrt{(z - z')^2 + \rho^2}} \quad (\text{A.6})$$

Radiated field

$$\vec{E} = jkZ[\hat{s} \times \hat{s} \times \vec{I}(\beta = \beta') + Y \hat{s} \times \vec{M}(\beta = \beta')] \frac{e^{-j\pi/4}}{\sqrt{8\pi k \sin \beta'}} e^{-jkz'_s \cos \beta'} \frac{e^{-jks}}{\sqrt{s}} \quad (\text{A.7})$$

At high frequencies, the radiation from the line sources, as derived here, yield the field in the direction of the diffracted cones (i.e Keller Cone $\beta = \beta'$).

References

- [1] J.B. Keller, "Geometrical Theory of diffraction," *J.Opt.Soc.Am.*, vol. 52, pp. 116-130, 1962.
- [2] R.G.Kouyoumjian and P.H.Pathak, "A uniform geometrical theory of diffraction for an edge in a perfectly conducting surface," *Proc. IEEE*, vol. 62, pp. 1448-1461, Nov. 1974.
- [3] C.E. Ryan and L.Peters, "Evaluation of the edge-diffracted fields including equivalent currents for the caustic regions," *IEEE Trans. AP.*, vol. AP-7, pp. 292-299, May 1969.
- [4] E.F.Knott and T.B.A. Senior, "Comparison of three high-frequency diffraction techniques," *Proc. IEEE*, vol. 62, pp. 1468-1474, Nov. 1974.
- [5] A.Michaeli, "Equivalent edge currents for arbitrary aspects of observation," *IEEE Trans. AP.*, vol. AP-32, no:3, March 1984.
- [6] R.J.Marhefka O.Merih Buyukdura and W.Ebihara, "Radar Cross Section Studies, phase 3," *The Ohio State University Electroscience Lab. Report*, no:716621-1, April 1986.
- [7] A.Michaeli, "Elimination of infinities in equivalent edge currents. part I:Fringe current components," *IEEE Trans. AP.*, vol. AP-34, no:7, July 1986
- [8] A.Michaeli, "Elimination of infinities in equivalent edge currents, part II: Physical optics components," *IEEE Trans. AP.*, vol. AP-34, no:8, August 1986
- [9] F.A.Sitka, "UTD analysis of electromagnetic scattering by flat plate structures," *Ph.D. dissertation, Ohio State University*, Columbus, 1981.
- [10] .A.Ross, "Radar cross section of rectangular flat plates as a function of aspect angle," *IEEE Trans. AP.*, vol. AP-14, pp.329-335, May 1966